ISSN: 2054-7404
Archives of Business Research; Vol. 14 No. 08 (2026) (70-114)
https://doi.org/10.14738/abr.1408.12150

Global Geopolitical Psychodynamics

K.E. Plokhotnikov

1. Faculty of Physics, M.V.Lomonosov Moscow State University, Leninskie Gory, Moscow 119991 Russia and Financial University under the Government of the Russian Federation

Abstract: This paper models global geopolitical psychodynamics. The globe's land surface is specifically divided into distinct regions called geopatoms. A single target space is defined for the entire ensemble of geopatoms. The target space is parameterized by the segment [0,1]. Three target points, marked with the numbers 0, 0.5, and 1, play a special role. The three listed target points define: the geopatoms' desire for individual existence for goal 0, for unification into large associations for goal 1, and in the absence of a desire for the first two goals for goal 0.5. All geopatoms in the ensemble are classified as geopatoms of goals 0, 0.5, and 1. To describe the individual behavior of individual geopatoms, as well as groups of geopatoms of an ensemble in the target space, a mathematical model of psyphysics, previously developed by the author, is used. In the target space, the movement of geopatoms is described in terms of "will", "freedom", "force" and "power", which are defined and calculated in the model of psyphysics. Using a computational experiment, we study various types of psychodynamics in the target space of low- and high-ranking geopatoms' associations. It is shown that all types of psychodynamics can be roughly divided into two categories: indefinitely lasting quasi-periodic movements and regimes in which geopatoms dynamics may cease. The presence of the latter mode fundamentally distinguishes psychodynamics from ordinary dynamics over time. The work calculates a single index for all states on the globe, which describes the relationship between psyphysics and geophysics in the structure of each state. A primary analysis of the values found is carried out, and a table of index values is provided for 171 countries and territories with other status.

Keywords: geopolitics, geophysics, psyphysics, psychodynamics, target space, geopatom, large (low) ranking cluster, will, freedom, force, power.

INTRODUCTION

Previously, the author developed mathematical models of geopolitics [1], and also formulated and calculated the concept of force in geopolitics [2]. Moreover, even earlier, including for the purposes of modeling global social dynamics, a mathematical model of psyphysics (Psyphysics: Towards a Theory of Operator-Device Interaction) was developed [3]. The psyphysics model made it possible to describe an arbitrary subject of historical-political dynamics in terms of "will", "freedom", "force", and "power". The four concepts are defined and calculated in the psyphysics model.

This mathematical model combines geopolitics with the psyphysical model. The psychodynamics of global geopolitics is understood as the movement of individual fragments of it, previously called geopatoms (GEOPolitical ATOMs), within a target space [4].

Each geopatom is believed to possess attributes of will, freedom, force, and power. The target space in which geopatoms are positioned is defined by a pair of global goals, called the “realm of freedom” and the “realm of necessity”. These two global goals are mutually exclusive; they exist in a mutual opposition characterized by a measure called force. This mathematical model primarily aims to study the psychodynamics of geopatoms in the target space with respect to these two global goals. In addition to geopatoms pursuing the goals of achieving the realms of freedom and necessity, there are also groups of “center” geopatoms who do not pursue the goals of the first two types.

HABITAT CAPACITY DENSITY

The author’s model of geopolitics introduced a central concept: “habitat capacity”. This concept allowed us to separate the political environment — represented by peoples, their population density, their territories of residence, and current political preferences — from geopolitics, which is determined by objective geophysical circumstances. Geopolitics encompasses climate, topography, the logistics of global trade flows, and the geopolitical confrontation between sea and continent — that is, everything that constitutes the material complex of conditions that accompanies the existence of the Earth’s inhabitants. This complex, to a significant extent, mediates the political behavior of the population. The model of geopolitics clarifies and generalizes the generally accepted geopolitical classification of territories in terms of their orientation and positioning, either toward the sea or toward the continent.

Let us define the capacity density of the habitat, h, which is a function of such climatic characteristics as the average annual temperature, T, and the average annual precipitation, Q. In the author’s previous works [1], the following functional dependence was considered:

$$h = h(T,Q) = e^{a_1 + a_2 |T/T_{\text{comfort}} - 1|^{\alpha} + a_3 |Q/Q_{\text{comfort}} - 1|^{\beta}}, \tag{1}$$

where a_1, a_2, a_3, α, β, T_{comfort}, Q_{comfort} are some constants.

The constants in formula (1) were estimated using real climate data taken from the website [5]. Suitable data for average annual temperature [6] and precipitation [7] (data dating back to 1995) were selected and presented as matrices of size 360×720, which corresponds to a latitude and longitude resolution of 0.5^0. Figure 1a shows the distribution of average annual temperature, and Figure 1b shows the distribution of average annual precipitation as three-dimensional surfaces in latitude – longitude coordinates.

Comfortable values of temperature, T_{comfort}, and precipitation, Q_{comfort}, were found using a weighted average procedure, where the Earth’s population density, given in the resource [8], served as weights. Based on the materials of this resource, Figure 2a is used to construct the surface of the common logarithm of the population density (for 2000), which was expressed in units of people/km^2. The map shows that the density varies from 0 to 10^4 people/km^2. It turned out that $T_{\text{comfort}} = 18.5775^0\text{C}$, $Q_{\text{comfort}} = 1200.2$ mm.

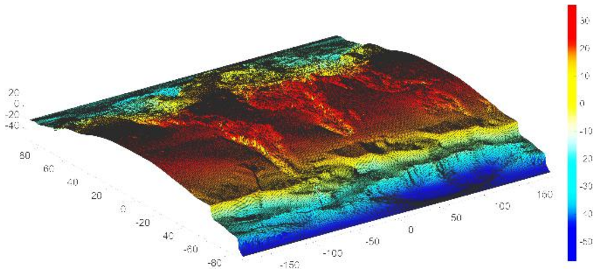

<u>Figure 1a</u>: Distribution surface of the average annual temperature in latitude - longitude coordinates (in degrees Celsius)

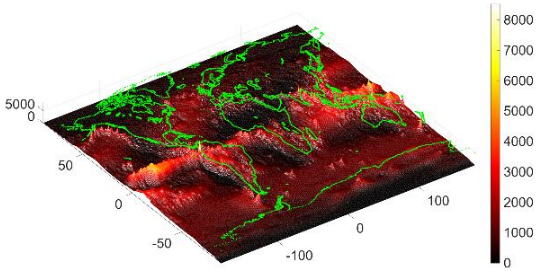

<u>Figure 1b</u>: Distribution surface of average annual precipitation in latitude-longitude coordinates (in millimeters)

Parameters a_1, a_2, and a_3 in formula (1) were calculated in the author's previous work, based on the fact that formula (1) defines a regression model for calculating the carrying capacity of a habitat. The results showed that $a_1 = 3.4189$, $a_2 = -1.6624$, and $a_3 = -1.4789$. The values for parameters α and β were also adjusted. It was assumed that $\alpha = 0.2$ and $\beta = 0.2$.

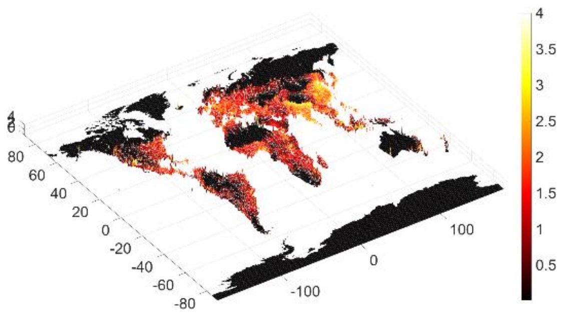

<u>Figure 2a</u>: Decimal logarithm of population density, expressed in units of people/km2

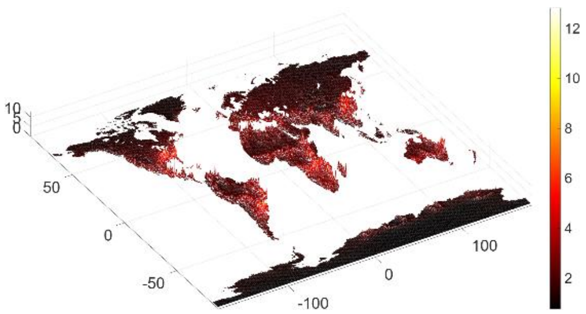

<u>Figure 2b</u>: Distribution of habitat capacity density in latitude-longitude coordinates

The resulting surface of the habitat capacity density, h, depending on latitude and longitude is shown in Figure 2b. The range of variation of the habitat capacity density was $[0{,}12.83]$. Note that the absolute values of the habitat capacity density are not important; only their ratios at different points on the Earth's surface are important.

Comparing the population density surfaces (Figure 2a) and habitat capacity density surfaces (Figure 2b) as a whole, their topographic similarity is noteworthy. This closeness was possible because the population density was logarithmized and subsequently found to be visually comparable to the habitat capacity density. This is also confirmed by the Pearson, Kendall, and Spearman correlation coefficients for the logarithmized population density and habitat capacity density, which are equal to 0.5789, 0.7610, and 0.9058, respectively.

The Spearman correlation coefficient has a particularly high value of 0.9058. Considering that the Spearman correlation coefficient is an indicator of the relationship between rank variables, the sought-after estimate of the capacity of the habitat (1), without taking into account the absolute values of the indicator, quite adequately describes the current population density of the Earth.

AN ARBITRARY CUT-UP OF THE LAND AREA OF THE EARTH'S SURFACE

Taking into account the capacity of the habitat, we "cut-up" the land area of the Earth's surface. Cutting refers to defining N land fragments. Generally, the number of fragments can vary from one to infinity, i.e., $N = 1, 2, \dots$ For $N = 1$, the entire land area of the Earth is considered to be a single fragment. This is a trivial case and will not be considered further, since with such a cut, we have no transport costs associated with exchange between territorial fragments. For this reason, we will henceforth assume that $N \geq 2$.

It should be noted that the arbitrary division into N fragments for $N \geq 2$ is a highly ambiguous procedure, as an infinite number of divisions with the same number of fragments, N, can exist. Against this backdrop of ambiguity in land area divisions, it is necessary to identify some stable, statistically invariant configurations of land area fragments. The aforementioned statistical search for invariant land area configurations involves the use of statistical trials or the Monte Carlo method.

Let's formulate an algorithm for randomly distributing N points on the land surface, taking into account the capacity of the habitat. We will define Voronoi polygons for each point. Using these polygons, we will consider one possible partition of the Earth's land surface.

Let us define N points within the habitat on the Earth's surface with coordinates $z_i = (\varphi_i, \lambda_i)$, $i = 1, \dots, N$, where φ_i is the latitude and λ_i is the longitude of the i-th point. In what follows, we assume that the latitude and longitude vary, respectively, either within the ranges $[-90^0, 90^0]$, $[-180^0, 180^0]$, or $-$ $[-\frac{\pi}{2}, \frac{\pi}{2}]$, $[-\pi, \pi]$, when degrees or radians are chosen when measuring angles. We will assume that all points are localized within the land area, which we will denote as $Land$.

Let each point z_i correspond to a certain region ω_i. Based on the above considerations, the global capacity of the environment,

$$U = \iint_{Land} d\varphi d\lambda \cdot \cos\varphi \cdot h(T(\varphi,\lambda), Q(\varphi,\lambda)), \tag{2}$$

can be rewritten as:

$$U = \sum_{i=1}^{N} u_i \, , u_i = \iint_{\omega_i} d\varphi d\lambda \cdot \cos\varphi \cdot h. \tag{3}$$

Taking into account (2), (3) it is clear that $Land = \bigcup_{i=1}^{N} \omega_i$, i.e. the set of regions $\{\omega_1, \dots, \omega_N\}$ determines a certain division into subregions of the entire land of the Earth's surface.

Let's take into account the fact that our data are determined on the Earth's surface with a resolution of 0.5^0. Considering that $\varphi_i = \frac{\pi}{180}(-89.75 + 0.5(i-1))$, $\lambda_j = \frac{\pi}{180}(-179.75 + 0.5(j-1))$, $i = 1, \dots, 360$, $j = 1, \dots, 720$, we can place a grid on the Earth's surface with nodes at the points $g_{i,j} = (\varphi_i, \lambda_j)$, $i = 1, \dots, 360$; $j = 1, \dots, 720$. There will be a total of such nodes $N_{Sphere} = 360 \times 720 = 259'200$. Among all the nodes of the N_{Sphere} grid, we select those that relate to land. Let the value N_{Land} denote the number of nodes of the grid that relates to land.

Let's introduce notations for the coordinates of points on the land surface: $z_k = (\varphi_k, \lambda_k)$, $k = 1, \dots, N_{Land}$. Using formula (1), we calculate the habitat capacity density h_k, $k = 1, \dots, N_{Land}$, at each of the selected land points. We determine the probabilities of randomly selecting each land point according to the following discrete distribution:

$$p_k = \frac{h_k \cos\varphi_k}{\sum_{l=1}^{N_{Land}} h_l \cos\varphi_l},\ k = 1, \dots, N_{Land}. \quad (4)$$

Distribution (4) is truly a discrete probability distribution, since $p_k \geq 0$, $k = 1, \dots, N_{Land}$ and $\sum_{k=1}^{N_{Land}} p_k = 1$. It turned out that $N_{Land} = 81'192$, while the ratio $N_{Land}/N_{Sphere} \cong 0.3132$ is slightly greater than the known ratio of land and ocean surfaces, equal to 0.292. This difference can be associated with the use of a fairly coarse grid of longitudes and latitudes with a resolution of 0.5^0.

Taking into account (4), we can use the Monte Carlo method to simulate the random positioning of N points within the land. To refine the random selection procedure, we define the cumulative probability of the discrete random variable (4) as a sequence $P_k = \sum_{l=1}^{k} p_l$, $k = 1, \dots, N_{Land}$, where $P_1 = p_1$,…, $P_{N_{Land}} = 1$.

Let us choose some uniformly random number ξ from the interval $[0,1]$, then it will correspond to the point number $k(\xi) \in \{1, \dots, N_{Land}\}$ according to the formula:

$$k(\xi) = \begin{cases} 1, \xi < P_1; \\ 2, P_1 \leq \xi < P_2; \\ \dots \\ N_{Land}, P_{N_{Land}-1} \leq \xi < P_{N_{Land}}. \end{cases} \quad (5)$$

As a result, taking into account (4), (5), an algorithm for generating a random set of N points $\{z_{k_1}, \dots, z_{k_N}\}$ from the set of available $\{z_1, \dots, z_{N_{Land}}\}$ is defined. In the general case, among a sample of N points $\{z_{k_1}, \dots, z_{k_N}\}$, some of them may be repeated. Considering that in the future the sample of points will not exceed the value of 10^4, i.e. $N \leq 10^4$, and $N_{Land} = 81'192 \gg 10^4 \geq N$, we will ignore possible repetitions of points in the sample.

Figure 3 shows an example of a random distribution of points on the land surface using the Monte Carlo method according to procedure (4), (5) and for $N = 5 \cdot 10^3$. The corresponding Voronoi polygons are plotted, taking into account the coastline and poles. Random points are depicted as blue dots, and the Voronoi polygons themselves are labeled with random colors.

The calculation, the results of which are shown in Figure 3, calculated the proportion of the Voronoi polygon area, S_{Land}, and the habitat capacity, U_{Land}, that are located on land. It turned out that $S_{Land} = 0.2897$, $U_{Land} = 6.1396$. Thus, the indicator for the proportion of land on the Earth's surface, $S_{Land} = 0.2897$, turned out to be close to the known indicator.

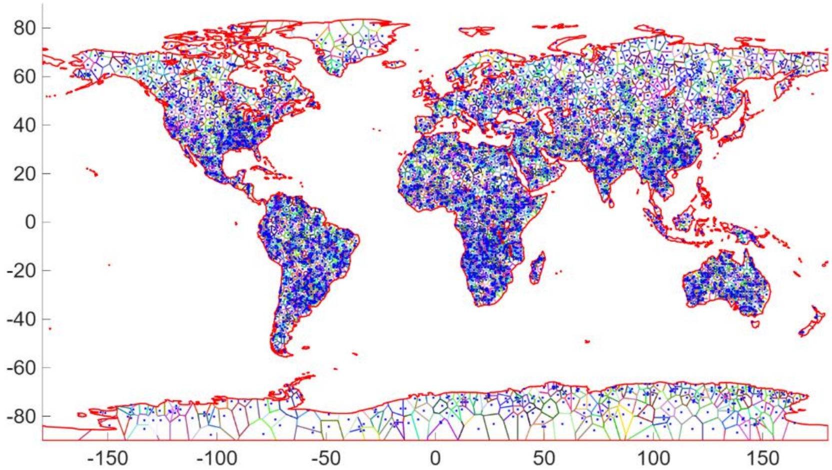

Figure 3: Map of the Earth's surface with a random set of $N = 5 \cdot 10^3$ points within the land and Voronoi polygons

DETERMINATION OF TRAFFIC BETWEEN TERRITORIES

Following [1,2], we define traffic between territories in relation to its energy costs. We introduce a "generalized distance" between territories, which takes into account the relief and the costs associated with overcoming it due to traffic.

First, we define costless traffic. We introduce the matrix $\{\alpha_{i,j}\}$, $i,j = 1,\dots,N$, whose elements characterize the transfer of a share of the i-th habitat capacity, u_i, to the j-th habitat capacity, u_j, due to traffic. The matrix $\{\alpha_{i,j}\}$, $i,j = 1,\dots,N$, acts as a measure of the exchange of habitat capacity between a set of territories associated with points $z_i = (\varphi_i, \lambda_i)$, $i = 1,\dots,N$, on the Earth's surface. According to the definition, it follows that

$$\sum_{j=1}^{N} \alpha_{i,j} = 1, \tag{6}$$

where $\alpha_{i,i}$ is the fraction of the i-th habitat capacity not subject to traffic, i.e., it is the fraction that remains within the i-th territory. The set of habitat capacities of territories u_i, $i = 1,\dots,N$, acts as a resource, which in the context of traffic is considered universal and additive.

Now, let us assume that when moving part of the habitat capacity from point i to point j, the share of resource $\gamma_{i,j}$ is lost due to traffic, and we assume that $0 \le \gamma_{i,j} \le 1, i \ne j;\ i,j = 1,\dots,N$. We assume that there are no costs within the logistics point, i.e. $\gamma_{i,i} = 0, i = 1,\dots,N$. We will call the matrix $\{\gamma_{i,j}\}, i,j = 1,\dots,N$, the matrix of transport costs. Taking into account (6), we compose a functional, Tr, of all transport costs:

$$Tr = 2\sum_{i=1}^{N} \sum_{j=1, j\ne i}^{N} \alpha_{i,j}\gamma_{i,j}u_i. \tag{7}$$

For further study of the transport cost functional (7), additional clarifications of the form of matrices $\{\alpha_{i,j}\}, \{\gamma_{i,j}\}, i,j = 1,\dots,N$ are required. Let us consider the so-called gravity model [9], which is well known in the theory of transport flows, in which a certain "generalized distance", $d_{i,j}$ ($d_{i,j} \ge 0$) is introduced between the i-th and j-th territories. Note that the distance matrix $\{d_{i,j}\}$, $i,j = 1,\dots,N$, generally speaking, is not symmetric, i.e. $d_{i,j} \ne d_{j,i}$, whereas by definition it is considered that $d_{i,i} = 0$, $i = 1,\dots,N$. Note that the condition $d_{i,j} = 0$ does not necessarily imply that the points z_i and z_j coincide in physical space.

Let us choose an exponential dependence of the coefficients of the matrices $\{\alpha_{i,j}\}$, $\{\gamma_{i,j}\}$, $i,j = 1,\dots,N$ on the generalized distance, then we can write the following representations:

$$\alpha_{i,j} = \frac{e^{-\beta d_{i,j}}}{\sum_{k=1}^{N} e^{-\beta d_{i,k}}},\ \gamma_{i,j} = \tfrac{1}{2} r(1 - e^{-\beta_2 d_{i,j}}), \tag{8}$$

where β, β_2, r are some non-negative parameters. A direct check can verify that condition (6) is satisfied for the matrix $\{\alpha_{i,j}\}$, $i,j = 1,\dots,N$ in form (8). According to (8), when $d_{i,j} = 0$, there are no transportation costs, i.e., $\gamma_{i,j} = 0$. Finally, when $\beta_2 \to \infty$ and when $d_{i,j} \neq 0$, it follows that $\gamma_{i,j} \to \frac{1}{2}r$, i.e., the share of transportation costs becomes a constant value equal to $\frac{1}{2}r$. From the last remark it follows that $0 \le r \le 2$.

Substituting (8) into (7), we find the following expression for the total costs of transport:

$$Tr = r \sum_{i=1}^{N} [1 - \sum_{k=1}^{N} e^{-(\beta+\beta_2)d_{i,k}} / \sum_{k=1}^{N} e^{-\beta d_{i,k}}] u_i. \tag{7′}$$

The following properties, which can be verified directly, are characteristic of transportation costs in the form (7′). First, when the distance between points becomes zero, i.e. $d_{i,j} = 0, i,j = 1,\dots,N$, there are no transportation costs, $Tr = 0$. Second, when the distance between points tends to infinity, i.e. $d_{i,j} \to \infty, i \neq j; i,j = 1,\dots,N$, the transportation costs, due to the chosen dependencies (8), also tend to zero, $Tr \to 0$. Note that a distance equal to zero or tending to infinity between a pair of points does not mean that the points merge or diverge to infinity.

Let us consider transport costs in the form (7′) as a function of the parameter β_2, i.e. $Tr = Tr(\beta_2)$. In this case, it is obvious that $Tr(0) \equiv 0$. Now let $\beta_2 \to \infty$, then $Tr(\beta_2) \to Tr(\infty) = r \sum_{i=1}^{N} [1 - 1/\sum_{k=1}^{N} e^{-\beta d_{i,k}}] u_i$. For the last functional of transport costs, it is obvious that the global minimum, equal to zero, is achieved only when the distances between points tend to infinity. It is the last version of the functional that will be considered further. In this case, the points will not converge; they will “repel” each other and fill the maximum of the habitat, since they are “locked” on the surface of the Earth’s sphere.

In the author’s works [1,2], the condition for the limit transition $\beta_2 \to \infty$ was called the “minimax transport doctrine”, which is deciphered according to the formula: minimum transport costs with maximum filling of the capacity of the habitat.

Taking into account the minimax transportation doctrine, the global traffic costs (7′) can be rewritten as:

$$Tr = \sum_{i,j=1}^{N} Tr_{i,j},\ Tr_{i,j} = r u_i \mathrm{A}_{i,j}, \tag{7″}$$

where $\mathrm{A}_{i,j} = \alpha_{i,j}(1 - \delta_{i,j})$ $i,j = 1,\dots,N$, $\delta_{i,j}$ is the Kronecker delta, i.e. $\delta_{i,i} = 1$, $\delta_{i,j} = 0$, when $i \neq j$. Note that, according to (7″), $Tr_{i,i} = 0$, since $\mathrm{A}_{i,i} = 0$, $i = 1,\dots,N$. It is obvious that the elements of the matrices $\{\mathrm{A}_{i,j}\}$, $i,j = 1,\dots,N$ coincide with the elements of the matrix $\{\alpha_{i,j}\}$, $i,j = 1,\dots,N$ except for the diagonal elements, where there are zeros.

The elements of the transport cost matrix $\{Tr_{i,j}\}$, $i,j = 1,\dots,N$ in (7″) have a transparent physical meaning. They represent the portion of the habitat capacity of the i-th territory that is spent on traffic to the j-th territory. Note that the habitat capacities of all land territories $\{u_i\}$, $i = 1,\dots,N$, act as a universal resource providing traffic between territories. As a result, for each i-th territory, we can construct a traffic cost vector $Tr_{i,:} = (Tr_{i,1},\dots,Tr_{i,N})$. We now turn to a brief presentation of the method for constructing the matrix of generalized distances $\{d_{i,j}\}$, $i,j = 1,\dots,N$.

CALCULATING THE GENERALIZED DISTANCE MATRIX

To determine the algorithm for calculating the distance matrix $\{d_{i,j}\}$, $i,j = 1,\dots,N$, we will express a number of physical considerations about the energy costs of moving one conventional unit of cargo weight from point $z_1 = (\varphi_1,\lambda_1)$ to point $z_2 = (\varphi_2,\lambda_2)$. Let the cargo movement route be defined as a line: $\varphi = \varphi(s)$, $\lambda = \lambda(s)$, $0 \le s \le l$. The line length, s, acts as an argument for parameterization of the line, varying from zero to its maximum value, l, equal to the route length, while it is assumed that $\varphi_1 = \varphi(0)$, $\lambda_1 = \lambda(0)$ and $\varphi_2 = \varphi(l)$, $\lambda_2 = \lambda(l)$.

Let the initial route be located entirely on the land surface. In this case, the energy cost of moving one conventional unit of cargo weight consists of three characteristic movement patterns: 1) vertical upward movement of the cargo due to terrain features; 2) vertical lowering of the cargo due to terrain features; 3) movement of the cargo along an inclined surface. The first two points of these movement patterns describe the energy costs of moving the cargo "up and down". The last point is characterized primarily by the energy costs of overcoming rolling friction within modes of transport such as road and rail. Let $Z = Z(\varphi,\lambda)$ be the land surface topography. Then, for the chosen route for moving a conventional unit of cargo mass, we can write the function $Z(s) = Z(\varphi(s),\lambda(s))$, $0 \le s \le l$.

Taking into account the stated physical considerations, we write a formula for calculating the generalized distance along the selected trajectory between a pair of points z_1 and z_2, d_{earth}:

$$d_{\text{earth}} = g_1 \int_0^l \frac{dZ}{ds}\kappa\left(\frac{dZ}{ds}\right)ds - g_2 \int_0^l \frac{dZ}{ds}\kappa\left(-\frac{dZ}{ds}\right)ds + g_3 \int_0^l \sqrt{1-\left(\frac{dZ}{ds}\right)^2}\,ds, \tag{9}$$

where $\kappa(t) = 1,\ t \ge 0$; $\kappa(t) = 0,\ t < 0$ is the so-called "unit" function. Parameters g_1, g_2, g_3 characterize the contribution of each type of motion to the displacement of one conventional unit of cargo mass. The integrals included in (9) are called transport integrals in the author's previous works.

Now let's assume that the route of one conventional unit of cargo mass lies entirely at sea, i.e., the departure and arrival points, as well as all other points along the route, lie on the sea surface. In this case, the energy costs of moving one unit of conventional cargo weight by sea transport are associated with overcoming viscous friction. To calculate the distance along the chosen trajectory between the pair of points z_1 and z_2, d_{sea}, we can use formula (9). We assume that the watercraft moves along a horizontal surface, for which we can assume that $dZ/ds = 0$. Taking into account the final integral in (9) and performing elementary integration, we write the corresponding transport integral as follows:

$$d_{\text{sea}} = g_4 l, \tag{10}$$

where g_4 is a non-negative parameter accounting for the averaged properties of viscous friction in the aquatic environment of the aggregate water transport.

Note that any route between a departure and destination point can be broken down into stages of travel solely by land or solely by sea. By applying either formula (9) or formula (10) to each stage and adding the resulting values, we find the final distance between the pair of points. Distances calculated using formulas (9) and (10) are not distances in the usual sense of the word. Rather, they act as effective distances, which can always be measured by calculating the average energy required to move one conventional unit of cargo mass from the departure point to the destination.

The considerations regarding the choice of values for the parameters g_1, g_2, g_3, g_4 were described in detail in the author's previous work [1], devoted to the mathematical modeling of geopolitics. We believe that

$$g_1 = 1,\ g_2 = 1,\ g_3 = 10^{-3},\ g_4 = 1.3639 \cdot 10^{-3}. \tag{11}$$

To calculate the generalized distance (9), (10) between an arbitrary pair of points on the Earth's surface $z_1 = (\varphi_1, \lambda_1)$, $z_2 = (\varphi_2, \lambda_2)$, we construct a full circumference of the Earth passing through the given pair of points. We assume that the full circumference lies in a plane passing through the center of the Earth. We define two-unit vectors $\boldsymbol{n}_1, \boldsymbol{n}_2$, which point to the pair of selected points $z_1 = (\varphi_1, \lambda_1)$, $z_2 = (\varphi_2, \lambda_2)$, then

$$\boldsymbol{n}_k = (\cos\lambda_k \cos\varphi_k\,, \sin\lambda_k \cos\varphi_k\,, \sin\varphi_k), k = 1{,}2. \tag{12}$$

Let a vector $\boldsymbol{n} = (n_x, n_y, n_z)$ of unit length point to an arbitrary point on a full circle passing through a chosen pair of points. It is clear that vector $\boldsymbol{n}$ lies in the plane formed by vectors $\boldsymbol{n}_1, \boldsymbol{n}_2$. Taking into account (12), after simple transformations, we find

$$\boldsymbol{n} = \boldsymbol{n}(s) = \frac{\sin(\theta - s)}{\sin\theta}\boldsymbol{n}_1 + \frac{\sin s}{\sin\theta}\boldsymbol{n}_2, \tag{13}$$

where θ is the angle between the pair of vectors $\boldsymbol{n}_1, \boldsymbol{n}_2$, and $(\boldsymbol{n}_1, \boldsymbol{n}_2) = \cos\theta$. According to (13), it is obvious that $\boldsymbol{n}(0) = \boldsymbol{n}_1$ and $\boldsymbol{n}(\theta) = \boldsymbol{n}_2$. The angle θ can be calculated using the formula:

$$\theta = \begin{cases} \pm\arccos(\boldsymbol{n}_1, \boldsymbol{n}_2)\,, (\boldsymbol{n}_1, \boldsymbol{n}_2) \geq 0; \\ \pm\pi \mp \arccos|(\boldsymbol{n}_1, \boldsymbol{n}_2)|\,, (\boldsymbol{n}_1, \boldsymbol{n}_2) < 0; \end{cases} \tag{14}$$

in further calculations, the upper sign was chosen.

Taking into account (13), and also considering that $\boldsymbol{n}(s) = (\cos\lambda(s)\cos\varphi(s)\,, \sin\lambda(s)\cos\varphi(s)\,,\ \sin\varphi(s))$, we find a parametric entry for the full circle in the "latitude – longitude" coordinates:

$$\varphi = \varphi(s) = \arcsin(n_z) = \arcsin[\tfrac{\sin(\theta - s)}{\sin\theta}\sin\varphi_1 + \tfrac{\sin s}{\sin\theta}\sin\varphi_2], \tag{15}$$

$$\lambda = \lambda(s) = \operatorname{arctg}\frac{n_y}{n_x} = \operatorname{arctg}\frac{\sin(\theta - s)\sin\lambda_1\cos\varphi_1 + \sin s \sin\lambda_2\cos\varphi_2}{\sin(\theta - s)\cos\lambda_1\cos\varphi_1 + \sin s\cos\lambda_2\cos\varphi_2}. \tag{15'}$$

Note that formula (15′) is true when $n_x > 0$. In the other two cases: 1) $n_x < 0, n_y > 0$; 2) $n_x < 0, n_y < 0$, π must be added and subtracted from the expression in (15′), respectively.

Let's construct a vector of unit length $\boldsymbol{n}_{dc}$, which indicates the intersection point of the full circle with the date line. We assume that vector $\boldsymbol{n}_{dc}$ lies in the same plane as vectors

$\boldsymbol{n}_1$ and $\boldsymbol{n}_2$. To do this, taking into account (15′), we must solve the equation $\lambda(s) = \pm\pi$ with respect to s. We need three roots $r_{dc} \in \{s_{dc}, s_{dc} \pm \pi\}$, where $s_{dc} = \operatorname{arctg} \frac{\sin\theta \sin\lambda_1 \cos\varphi_1}{\cos\theta \sin\lambda_1 \cos\varphi_1 - \sin\lambda_2 \cos\varphi_2}$. Either the first root, or the second and third ones, are chosen, for which $n_x(r_{dc}) < 0$. Between the second and third roots, the choice is made in favor of the value with the minimum absolute value. In this case, the desired vector, $\boldsymbol{n}_{dc}$, pointing to the date line, is determined according to the equation $\boldsymbol{n}_{dc} = \boldsymbol{n}(r_{dc})$.

The small and large fragments of a circle passing through a given pair of points and the center of the Earth are described by formulas (12) – (15′), when the parameter s takes values from the segments $[0, \theta]$ and $[\theta, 2\pi]$ (or $[-2\pi + \theta, 0]$), respectively. Figure 4 shows a graphical example of the positioning of two random vectors $\boldsymbol{n}_1, \boldsymbol{n}_2$ and the corresponding date change vector $\boldsymbol{n}_{dc}$. The small and large fragments of the circle are marked with markers in the form of a set of pentagrams and hexagrams, respectively. Examples of two cases are given when the date change vector falls on the large (Figure 4a) and small (Figure 4b) fragments of the circle, respectively. From the point of view of the parameter s, the date change vector $\boldsymbol{n}_{dc}$ falls on the large fragment of the circle when $r_{dc} \notin [0, \theta]$ and, conversely, falls on the small fragment of the circle when $r_{dc} \in [0, \theta]$.

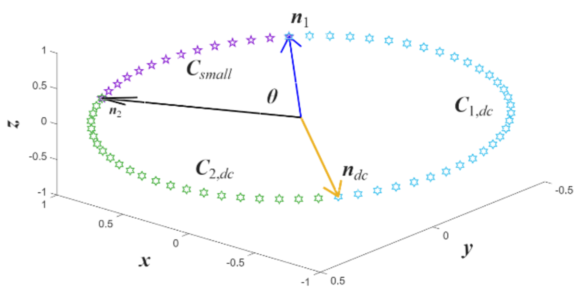

Figure 4a: The date change vector falls on a large fragment of the circle

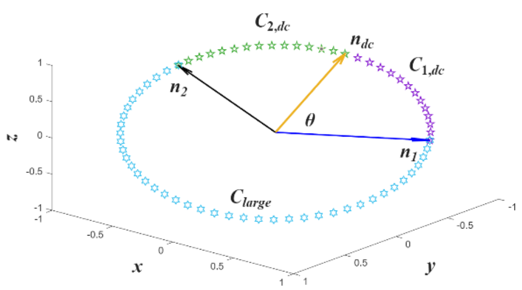

Figure 4b: The date change vector falls on a small fragment of the circle

Vectors $\boldsymbol{n}_1, \boldsymbol{n}_2$, $\boldsymbol{n}_{dc}$ divide the large circle into three parts. Let us assemble the small and large fragments of the large circle from the three specified parts. Let C, C_{small}, C_{large} denote the sets of points lying on the entire circle, as well as on its small and large fragments, respectively. In this case, by definition, $C = C_{small} \cup C_{large}$, where $C_{small} = \{\boldsymbol{n}(s) | s \in [0, \theta]\}$, $C_{large} = \{\boldsymbol{n}(s) | s \in [\theta, 2\pi]\}$. Taking into account Figure 4, we should consider two cases of assembling small and large fragments of the entire circle from the specified three parts:

$$\begin{cases} C_{small}, C_{large} = C_{1,dc} \cup C_{2,dc}, r_{dc} \notin [0, \theta]; \\ C_{small} = C_{1,dc} \cup C_{2,dc}, C_{large}, r_{dc} \in [0, \theta]; \end{cases} \tag{16}$$

where $C_{1,dc}$, $C_{2,dc}$ are arcs of circle C between pairs of vectors $\boldsymbol{n}_1, \boldsymbol{n}_{dc}$ and $\boldsymbol{n}_2, \boldsymbol{n}_{dc}$, respectively.

Figure 5a shows an example of positioning $N = 50$ points on the land surface. The points were chosen randomly according to the algorithm in section #3, i.e., taking into account the carrying capacity density of the habitat. All large circles, numbering $\frac{50 \times 49}{2} =$

$1'225$, are constructed connecting each pair of points. Furthermore, the circles are marked according to their land (solid black line) and sea (dashed blue line).

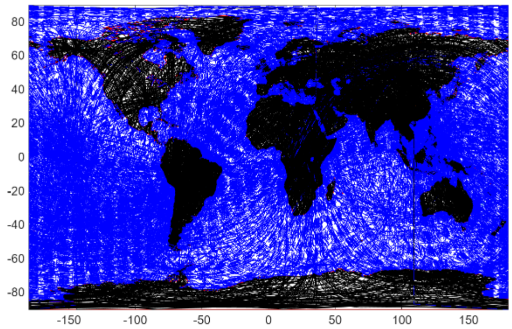

Figure 5a: Projection onto the "latitude - longitude" rectangle of great circles connecting $N = 50$ points in pairs

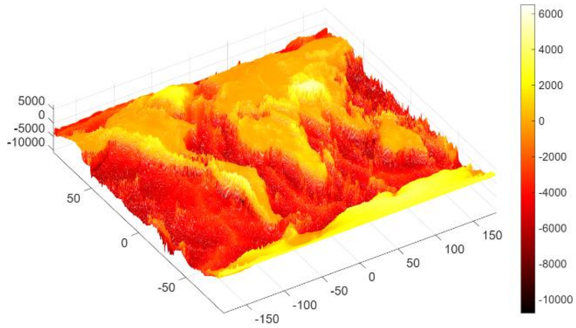

Figure 5b: Relief map of the Earth's surface

According to formula (9), to calculate the effective distance for moving one conventional unit of cargo mass on the Earth's surface, it is important to know the derivative of the relief $Z = Z(\varphi, \lambda)$ along the route described by a certain trajectory. Figure 5b shows a map of the Earth's surface relief in latitude-longitude coordinates. Let, for example, a route be laid between a pair of points $z_1 = (\varphi_1, \lambda_1)$, $z_2 = (\varphi_2, \lambda_2)$ such that $\varphi = \varphi(s), \lambda = \lambda(s)$, where s is the parameter describing the path traveled from the starting point. In this case, it is obvious that $\frac{dZ}{ds} = \frac{\partial Z}{\partial \varphi}\frac{d\varphi}{ds} + \frac{\partial Z}{\partial \lambda}\frac{d\lambda}{ds}$.

As a route between a pair of points on the surface of the Earth's sphere, we sequentially select both fragments (small and large) of a full circle passing through the pair of points. A suitable trajectory is represented by formulas (15), (15′). It remains to find the derivatives. After simple calculations, we obtain:

$$\frac{d\varphi}{ds} = \frac{-\cos(\theta - s)\sin\varphi_1 + \cos s \sin\varphi_2}{\sqrt{\sin^2\theta - [\sin(\theta - s)\sin\varphi_1 + \sin s \sin\varphi_2]^2}}, \quad (17)$$

$$\frac{d\lambda}{ds} = \frac{\sin\theta \sin(\lambda_2 - \lambda_1)\cos\varphi_1 \cos\varphi_2}{\sin^2\theta - [\sin(\theta - s)\sin\varphi_1 + \sin s \sin\varphi_2]^2}. \quad (17')$$

Let us introduce the distance matrix $D = \{d_{i,j}, i,j = 1, \dots, N\}$ between all pairs of points. Let us define similar distance matrices found for small $D_{\text{small}} = \{d_{\text{small},i,j}, i,j = 1, \dots, N\}$ and large $D_{\text{large}} = \{d_{\text{large},i,j}, i,j = 1, \dots, N\}$ fragments of the arcs of the corresponding full circles. Taking into account the prospect of minimizing traffic costs, we assume that the sought-for distance matrix D is the elementwise minimum of the pair of distance matrices D_{small} and D_{large}, i.e. $D = \min(D_{\text{small}}, D_{\text{large}}) = \{d_{i,j} = \min(d_{\text{small},i,j}, d_{\text{large},i,j})\}$, $i,j = 1, \dots, N$.

To calculate the transport integrals in (9), we need the partial derivatives $\frac{\partial Z}{\partial \varphi}$ and $\frac{\partial Z}{\partial \lambda}$, which we calculate using finite differences with a relief resolution of 0.5^0 according to the formulas:

$$\left(\frac{\partial Z}{\partial \varphi}\right)_{i,j} = \frac{60}{\pi}(Z_{i+1,j} + Z_{i+2,j} - Z_{i-1,j} - Z_{i-2,j}), \quad (18)$$

where $i = 1, \dots, 360$; $j = 1, \dots, 720$ and

$$\left(\frac{1}{\cos\varphi}\frac{\partial Z}{\partial \lambda}\right)_{i,j} = \frac{60}{\pi \cos\varphi_i}(Z_{i,j+1}+Z_{i,j+2}-Z_{i,j-1}-Z_{i,j-2}), \quad (18')$$

where $i = 1, \dots, 360$; $j = 1, \dots, 720$, while in (18′) a periodic continuation by index j with a period of 720 is assumed.

The ordinary derivatives $\frac{d\varphi}{ds}$ and $\frac{d\lambda}{ds}$ were found according to (17), (17′). Otherwise, the fragment of the full circle connecting the pair of points was divided into parts passing separately on land and at sea. For each part, a suitable finite-difference grid was constructed with a number of nodes adapted to the length Δs of the selected part of the full circle according to the formula $2 + [n\Delta s]$. In the latter formula, the parameter n was typically chosen in the vicinity of 15, and $[\dots]$ was understood to be the integer part of the number.

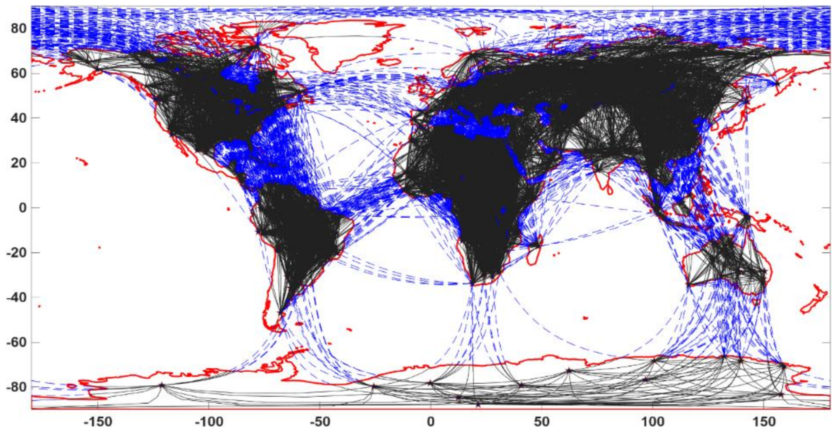

Figure 6: An example of positioning $N = 350$ points (markers in the form of pentagrams) within the land, as well as small fragments of large circles

Figure 6 shows an example in which $N = 350$ points were randomly placed within the land area according to the algorithm in section #3. Some of the minimal fragments of great circles passing through the corresponding pair of points were constructed. In the current calculation, the values of the elements of the distance matrix D varied in the range $[1.19 \cdot 10^{-5}, 0.0092]$. Note that the relief matrix Z used in formulas (18), (18′) was divided by the Earth's radius.

Note that almost always $d_{small,i,j} \le d_{large,i,j}$, $i,j = 1, \dots, N$. Taking into account all $\frac{1}{2}N(N-1)$ possible binary relationships, this inequality was not satisfied in $\cong 2.81\%$ of cases.

CALCULATION AND ANALYSIS OF THE TRANSPORT COST MATRIX

Formula (7′′) contains an expression for calculating the value of transport costs $\{Tr_{i,j}\}$, $i,j = 1, \dots, N$. This expression includes an undefined parameter β. To estimate it, we introduce a set of vectors $Tc_i = Tr_{i,:}$, $i = 1, \dots, N$, which characterize the individual profile of traffic costs for each region (Voronoi polygons). The set of vectors $Tc_1, \ldots, Tc_N$ are the rows of the transport cost matrix $\{Tr_{i,j}\}$, $i,j = 1, \ldots, N$. We calculate the matrix of correlation coefficients $\{Cr_{i,j}\}$, $i,j = 1, \ldots N$ of vectors Tc_i, $i = 1, \ldots, N$, i.e. $Cr_{i,j} = Corr(Tc_i, Tc_j)$, $i,j = 1, \ldots, N$, where the function $Corr(Tc_i, Tc_j)$ returns the Pearson correlation coefficient between the pair of vectors Tc_i and Tc_j.

Taking into account that the Pearson correlation coefficient is invariant with respect to the linear transformation of the data vectors, it turns out that the matrix of correlation coefficients does not depend on the product ru_i, $i = 1, \ldots, N$ and can be represented as: $Cr_{i,j} = Corr(\mathrm{A}_{i,:}, \mathrm{A}_{j,:})$, $i,j = 1, \ldots, N$. According to the definition in (7″), $\mathrm{A}_{i,j} = \alpha_{i,j}(1 - \delta_{i,j})$, where the vectors $\mathrm{A}_{i,:}$, $i = 1, \ldots, N$ are understood as the rows of the matrix $\{\mathrm{A}_{i,j}\}$, $i,j = 1, \ldots, N$.

We assume the future prospect of uniting individual regions into larger associations. The criterion for forming large territorial associations is the proximity of individual traffic cost profiles. We will consider the Pearson correlation coefficient as a measure of proximity. We will calculate the number of binary correlations $N_{corr} = \sum_{1=i<j=N}(Cr_{i,j} \geq 0.7)$ exceeding the threshold of 0.7, above which the correlation is considered high. We will calculate and plot the value of N_{corr} as a function of the parameter β. It turns out that the function $N_{corr} = N_{corr}(\beta)$ has a maximum. In other words, the set of vectors $Tc_1, \ldots, Tc_N$ is maximally correlated at some value $\beta = \beta_{max}$, at which the number of high binary correlation coefficients reaches a maximum $N_{corr,max} = \max_{\beta} N_{corr}(\beta)$.

Figure 7a shows a map of highly correlated pairs of points connected by lines. For these pairs, the correlation coefficients exceeded 0.92. Figure 7b shows a graph of the $N_{corr}(\beta)$ function versus β. In the presented calculation, it was assumed that $N = 10^3$, and $\beta_{max} = 340$, $N_{corr,max} = 72'179$, was found. The optimal value of the β_{max} parameter is marked with a red star in Figure 7b. Note that there are a total of $\frac{1}{2}N(N-1)|_{N=10^3} = 499'500$ binary correlations. The relative number $\frac{N_{corr,max}}{\frac{1}{2}N(N-1)}$ of highly correlated connections amounted to 14.45% in percentage.

According to the map in Figure 7a, the closeness of individual traffic costs for selected points in the following regions in descending order is clearly expressed: Africa, South America, North America, etc.

To aggregate land points into associations, we will use cluster analysis. As a measure of the proximity of a pair of points according to traffic profiles, we will choose the so-called "Pearson distance" $\rho_{i,j} = 1 - Cr_{i,j}$, $i,j = 1, \ldots, N$. The Pearson distance takes values from the interval $[0,2]$, and the closer the correlation coefficient is to unity, the smaller the Pearson distance. Figure 8a shows an example of a histogram of the distribution of binary Pearson distances $\rho_{1,2}, \rho_{1,3}, \ldots, \rho_{N-1,N}$ for $N = 10^3$. It is clearly seen that the binary Pearson distance is bimodal.

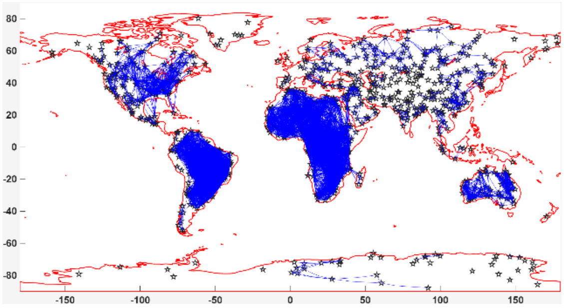

Figure 7a: Map of highly correlated pairs of points

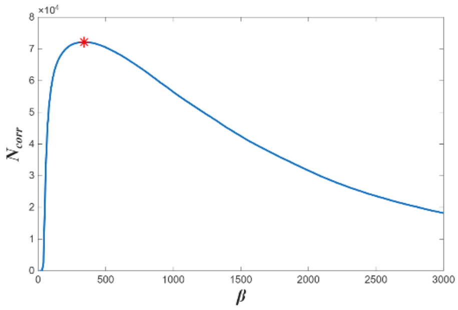

Figure 7b: Graph of the dependence of the function $N_{corr}(\beta)$ on β

As is known from the theory (algorithm) of cluster analysis [10], within the framework of the agglomerative procedure for cluster formation, we start with individual observations, which are considered as the initial atomic clusters. Then, in our case, using the Pearson distance, we find a pair with a minimal distance between them, these clusters are combined into a new composite cluster. Then the procedure is repeated; not only atomic clusters, but also composite ones can participate in it. The distance d_{c_1,c_2} between composite clusters $c_1 = \{i_1, \dots, i_r\}$, $c_2 = \{j_1, \dots, j_t\}$ is calculated using the average formula $d_{c_1,c_2} = \frac{1}{rt}\sum_{k=1}^{r}\sum_{l=1}^{t}\rho_{i_k,j_l}$, where r, t is the number of atomic clusters in each of the two composite ones. Ultimately, step by step, we arrive at a single, composite cluster. From now on, by cluster rank m we will mean the number of atomic clusters that comprise it.

Let us introduce the function of the number of clusters $N_{cl} = N_{cl}(m, d_{c_1,c_2})$, which depends on two variables: 1) m – the cluster rank and 2) d_{c_1,c_2} – the distance between clusters. It is clear that both the function N_{cl} itself and the variable m can take values from the set $\{1,2,\dots,N\}$. Figure 8b shows an example of the function $N_{cl} = N_{cl}(m, d_{c_1,c_2})$, constructed for the case of $N = 10^3$. Separate graphs in Figure 8b correspond to the dependence of N_{cl} on the distance d_{c_1,c_2} for different cluster ranks, $m = 1,2,\dots,N = 10^3$.

Let us define the number of one- and two-rank clusters $N_{1,2} = N_{cl}(1, d_{c_1,c_2}) + N_{cl}(2, d_{c_1,c_2})$. The selection of one- and two-rank clusters is related to the fact that it is impossible to construct a bordering polygon for each of them. From this point of view, their contribution will be considered small, while the number of large-rank clusters should be as noticeable as possible. Let us assume that the number of one- and two-rank clusters is $f_r N$, i.e. $N_{1,2} = f_r N$. Let us further choose the following value for the proportion, f_r of one- and two-rank clusters – 0.0135, i.e. $f_r = 0.0135$ or 1.35% in percent.

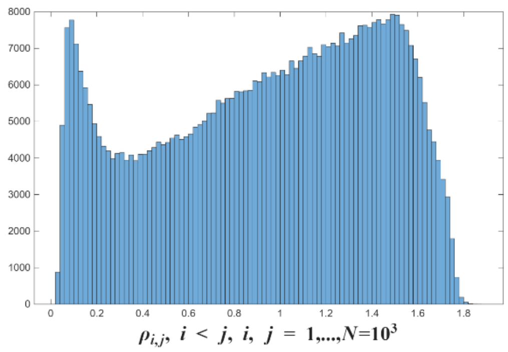

Figure 8a: Histogram of Pearson distances

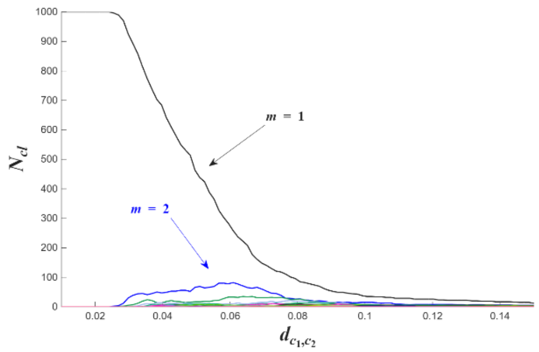

Figure 8b: Dependence $N_{cl} = N_{cl}(m, d_{c_1,c_2})$

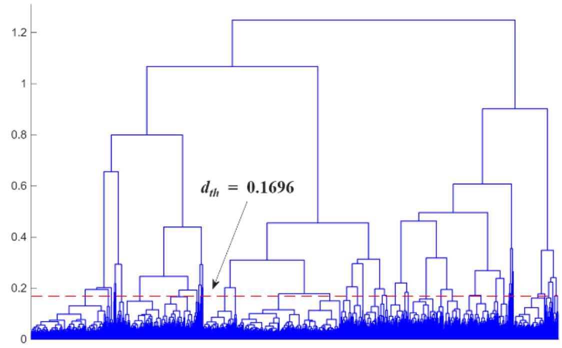

Figure 8c: Dendrogram of cluster analysis

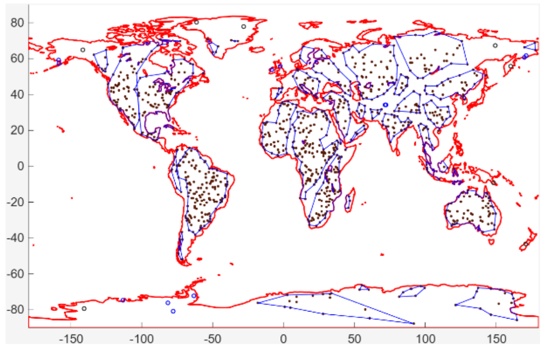

Figure 8d: Example of using cluster analysis

Figure 8c shows an example of a cluster analysis dendrogram for the case of $N = 10^3$. It also shows a straight dotted line determined by the distance between clusters $d_{th} = 0.1696$. The distance d_{th} is found from the condition that $N_{1,2} = f_r N$, $f_r = 0.0135$. Taking into account the graph in Figure 8b, the dependence of the number of peer clusters on d_{c_1,c_2} is a monotonically decreasing function, so it is always possible to find a suitable value of d_{th} for a given value of f_r.

Fixing the distance d_{th} determines the desired cluster classification of land surface points. Figure 8d shows the result of applying cluster analysis to the traffic cost matrix with an intercluster distance cutoff value of $d_{th} = 0.1696$ and $N = 10^3$. Figure 8d contains clusters of various ranks, starting with clusters of ranks one and two (markers in the form of circles). Large-scale clusters with three or more atomic clusters are highlighted using border polygons.

CLASSIFICATION OF REGIONS ON A SMALL-LARGE RANK SCALE

To classify regions of the Earth's surface into low-ranking and high-ranking regions, we will conduct several calculations similar to those shown in Figure 8d. Each calculation involves using cluster analysis to classify points on the land surface, randomly distributed according to the procedure in section #3. Clearly, each calculation will yield its own clustering map. It is necessary to somehow find the average clustering map.

Let S calculations of the transportation cost matrix $Tr^{(s)}$, $s = 1, \ldots, S$, be performed for some N. In each of the S calculations, N points on the land surface are positioned randomly according to the algorithm of section #3. We apply the clustering procedure Cl according to section #6 to each of the transportation cost matrices $\{Tr^{(1)}, \dots, Tr^{(S)}\}$. We choose some value of the parameter f_r that determines the proportion of the number of one- and two-rank clusters in relation to all selected points N. Applying the clustering procedure to the transportation cost matrix $Tr^{(s)}$ generates a set of clusters $\{\mathrm{K}_1^{(s)}, \dots, \mathrm{K}_{\kappa_s}^{(s)}\}$ of the original points, i.e. $Cl: Tr^{(s)} \to \{\mathrm{K}_1^{(s)}, \dots, \mathrm{K}_{\kappa_s}^{(s)}\}$.

Let us depict a set of clusters $\{\mathrm{K}_1^{(s)}, \dots, \mathrm{K}_{\kappa_s}^{(s)}\}$, $s = 1, \dots, S$, together with the coastline. Clusters of ranks one and two are depicted as markers in the form of circles. Clusters of rank three and higher are depicted using bordering polygons. Other points on the land surface are depicted as markers in the form of dots. Figure 9 shows an example of a map on which all possible clusters are concentrated. It was assumed that $f_r = 0.0135$, $N = 10^3$, $S = 24$. The cluster of lines in Figure 9 clearly demonstrates the presence of large-rank clusters.

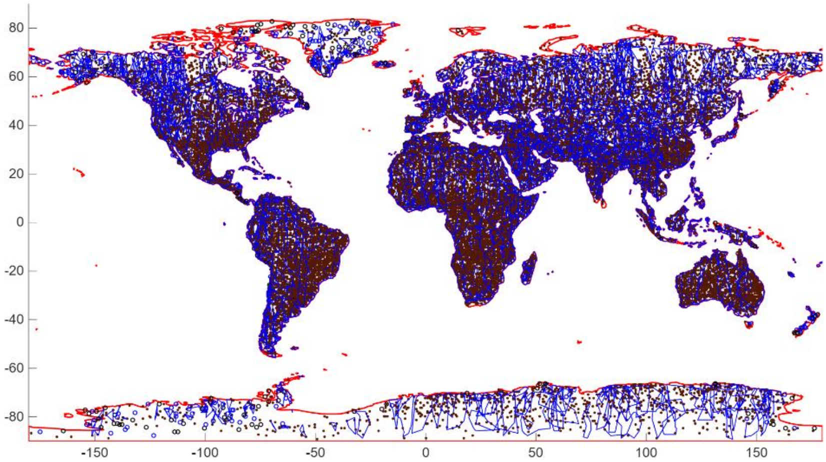

Figure 9: Cluster map, in the form of a set of bordering polygons

For a more detailed cutting of the land area, it is necessary to make a number of assumptions and calculations. In section #3, as part of the global procedure for marking the surface of the globe "latitude – longitude", a 360×720 grid was selected. It turned out that the number of grid nodes, N_{Land}, located on land was $N_{Land} = 81'192$. Let $z_l = (\varphi_l, \lambda_l)$ be the position of the l-th point on the land surface, $l = 1, \dots, N_{Land}$. For each cluster $\mathrm{K}_\kappa^{(s)}$, the rank of which is three or more, we construct a bordering polygon $B[\mathrm{K}_\kappa^{(s)}]$, $\kappa = 1, \dots, \kappa_s$, $s = 1, \dots, S$. Due to the choice of a small value of the parameter f_r, clusters of rank 1 and 2 will be ignored, since their contribution is small. Visually noticeable numbers of single- and double-rank clusters are concentrated in the polar regions.

For each land point z_l, $l = 1, \dots, N_{Land}$, we calculate the weight w_l, which is the sum of the number of occurrences of the l-th point in all polygon-shaped clusters of all statistical experiments on estimating transport cost matrices with subsequent use of cluster analysis, i.e.

$$w_l = \sum_{s=1}^{S} \sum_{\kappa=1}^{\kappa_s} (z_l \in B[\mathrm{K}_\kappa^{(s)}]),\ l = 1, \dots, N_{Land}, \quad (19)$$

where the parentheses $(z_l \in B[\mathrm{K}_\kappa^{(s)}])$ return one if the inclusion $z_l \in B[\mathrm{K}_\kappa^{(s)}]$ is true and zero if the opposite is true, i.e. $z_l \notin B[\mathrm{K}_\kappa^{(s)}]$.

The set of weights $W = \{w_1, \dots, w_{N_{Land}}\}$ will allow us to separate from each other regions that, on the one hand, are close to each other in terms of their individual traffic cost profiles, and on the other hand, a conservative component in the form of memory of belonging to certain groups of clusters in the set of statistical tests S will be taken into account. In formula (19), the contribution of the l-th point to each of the clusters is the same and equal to one.

Figure 10 shows two maps of the weight set W constructed using the same data in two-dimensional and spatial formats. When calculating the weight using formula (19), it was assumed that $f_r = 0.0135$, $N = 10^3$, $S = 24$, while ignoring the contribution of single- and dual-rank clusters. Visually, the maps in Figure 9 and Figure 10 are similar. Clusters of similar traffic cost profiles in Figure 10b are clearly visible as corresponding “towers” with flat tops. In the author’s work [2] 24 such towers can be distinguished; they are called “imperial towers”.

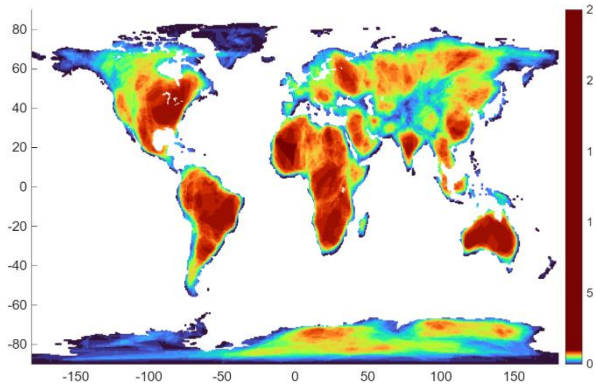

Figure 10a: Map of the set of weights in flat format

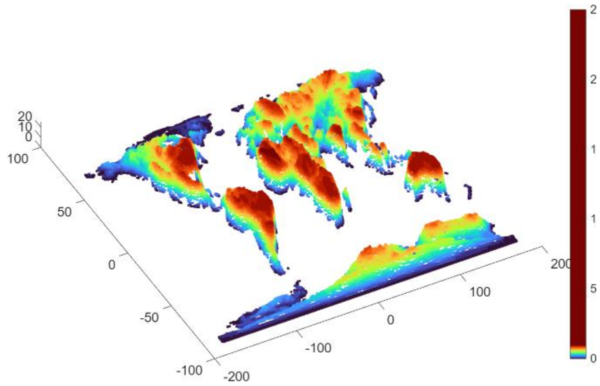

Figure 10b: Map of the set of weights in spatial format

Let us divide the set of weights (19) by the maximum value, i.e. introduce the normalization $W \to W / \max\limits_{1 \le l \le N_{Land}} w_l$. After normalization, the weight $W = \{w_l\}$, $l = 1, \dots, N_{Land}$ will vary in the range $[0,1]$ and will not directly depend on the number of statistical experiments S.

The ratio of certain territories to low-rank and high-rank ones is characterized by a weight normalized to the interval $[0,1]$. When $w_l \sim 0$, the l-th territory is considered to be a low-rank territory. When $w_l \sim 1$, the l-th territory is considered to be included in a high-rank cluster. Within the framework of the above remarks, one can define the force, F, as a weighted average sum of squared deviations from the weighted average value, i.e. the weighted average variation of the weight values, namely,

$$F = \frac{\sum_{l=1}^{N_{Land}} \cos\varphi_l \cdot (w_l - \bar{w})^2}{\sum_{l=1}^{N_{Land}} \cos\varphi_l}, \quad \bar{w} = \frac{\sum_{l=1}^{N_{Land}} \cos\varphi_l \cdot w_l}{\sum_{l=1}^{N_{Land}} \cos\varphi_l}, \tag{20}$$

where $\bar{w}$ is the weighted average value of the set of weights $W = \{w_l\}$, $l = 1, \ldots, N_{Land}$. The presence of the cosine of latitude in (20) takes into account the sphericity of the Earth's surface.

The value (20) could be called a global single-cluster force estimator. It measures the absence or presence of consolidation of atomic clusters into large-scale associations due to the proximity or distance of individual traffic cost profiles. Force F was calculated for the entire globe and found to be $F \cong 7063.55$.

Figure 11a shows the normalized weight level lines. Red dot markers indicate local weight maxima. Group clusters of red dots characterize the plateau-like geometry of the profiles. In Figure 11a, 5881 local maxima are marked by red dots, and $N_{lm} = 891$ black plus-shaped markers indicate the centers of clusters of local maxima.

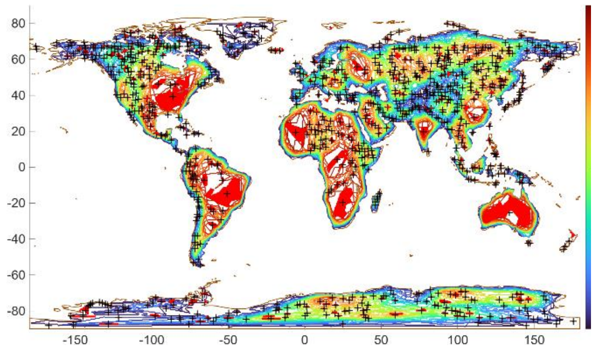

Figure 11a: Level lines of a set of weights: local maxima (red dots), centers of clusters of local maxima (black pluses)

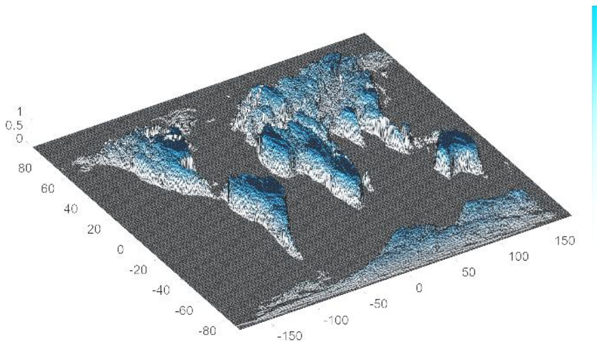

Figure 11b: Three-dimensional image of the normalized weight function

The presence of the geometry of the normalized weight function in the form of plateau profiles is clearly visible on the map in Figure 11b, similar to the map in Figure 10b, made in three-dimensional format.

We assume that the number of clusters is equal to the number of centers of local maxima clusters, $N_{lm} = 891$. For the distance between a pair of points, we consider the distance on the Earth's sphere as an angle θ, the formula for calculating which is given in (14). We find the smallest distance from the current point to the points of the selected set of centers, $N_{lm} = 891$ local maxima. The resulting minimum distance allows us to assign the current point to the corresponding point of the center of local maxima.

Figure 12 shows two maps in which all N_{Land} land points are classified according to the specified procedure. In Figure 12a, individual homogeneity polygons $N_{lm} = 891$ are filled with random colors. In Figure 12b, individual homogeneity polygons are filled with a color from a special palette, taking into account the weighted average value within each polygon. Note that in Figure 12, it is not the polygons that are colored, but rather clusters of land points assigned to a particular neighborhood of the centers of local maxima.

Roughly speaking, in Figure 12b, the red-brown color denotes regions that prefer high-ranking affiliations, while the blue-violet color denotes low-ranking affiliations. Note also that in many places, the coastline adjacent to high-ranking regions is colored blue, indicating affiliation with low-ranking clusters. This contrast significantly influences the force parameter.

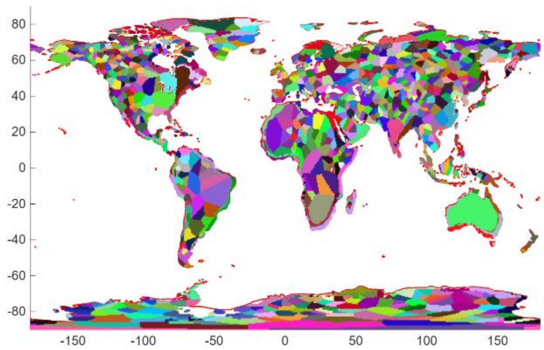

Figure 12a: Homogeneity polygons colored with random colors

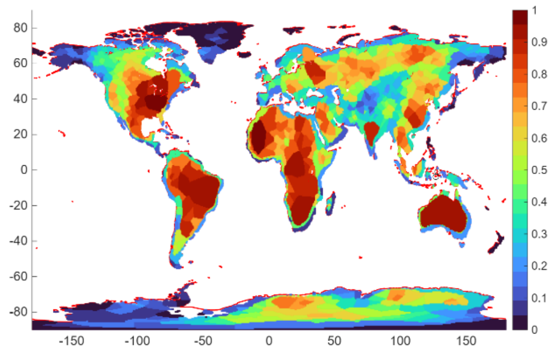

Figure 12b: Homogeneity polygons are colored with a color from the palette taking into account the weight value

Let us calculate the total square deviation of points from cluster centers, f. Let the above procedure result in $\mathrm{K}_1, \mathrm{K}_2, \dots, \mathrm{K}_\kappa$ clusters, each containing $n_1, n_2, \dots, n_\kappa$ points. Then the total square deviation of the points from the cluster centers, or the force in our terminology, can be calculated using the formula:

$$f = \sum_{i=1}^{\kappa} \frac{\sum_{j=1}^{n_i} \cos\varphi_j \cdot \left(w_{i,j} - \bar{w}_i\right)^2}{\sum_{j=1}^{n_i} \cos\varphi_j}, \quad \bar{w}_i = \frac{\sum_{j=1}^{n_i} \cos\varphi_j \cdot w_{i,j}}{\sum_{j=1}^{n_j} \cos\varphi_j}, \tag{21}$$

where $w_{i,j}$ is the weight of the j-th point of the i-th cluster, $j = 1, \dots, n_i$, $i = 1, \dots, \kappa$, $\bar{w}_i$ is the weighted mean center of the i-th cluster. In the calculations, the results of which are shown in Figure 12, it was assumed that $\kappa = N_{lm} = 891$, while it turned out that $f = 511.36$. The latter value is 13.81 times smaller than the single-cluster estimate $F = 7063.55$. Thus, the global force parameter can be significantly reduced taking into account local characteristics of traffic costs.

Ultimately, we can conclude that the force parameter, as a measure of the opposition between low-rank and high-rank clusters, is an objective characteristic. Force is built into the traffic cost infrastructure and is generated by the entire geophysical system: climate in terms of temperature and precipitation, topography, and traffic.

In the future, we will need to classify geopatoms into two or three groups. A two-group classification divides the geopatom ensemble into low-ranking and high-ranking geopatoms, respectively. Or, in another nomenclature, two groups of geopatoms are oriented toward constructing the realms of freedom and necessity. A three-group classification introduces another group, the “center” geopatoms, which distance themselves from constructing the realms of freedom and necessity. We will conditionally assign low-ranking geopatoms to target 0, high-ranking geopatoms to target 1, and center geopatoms to target 0.5. Thus, all possible targets will be concentrated on the interval $[0,1]$. The reason for this will become clear from the further exposition of the mathematical model of psyphysics.

To classify geopatoms into corresponding target groups, we will use cluster analysis. Figure 8c already showed the results of using cluster analysis. In both cases, the k-means method was used to divide the geopatom ensemble. The average geopatom weight $\overline{w}_i$, $i = 1, \dots, N_{lm} = 891$, presented in (21), was used as the classification variable. Figure 13 shows the result of dividing the geopatom ensemble into two groups (Figure 13a) and three groups (Figure 13b), respectively.

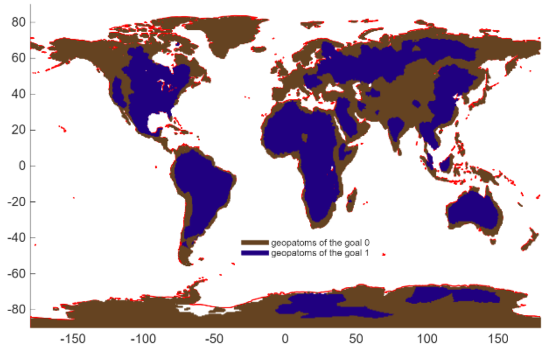

Figure 13a: Division of the geopatoms ensemble into two groups

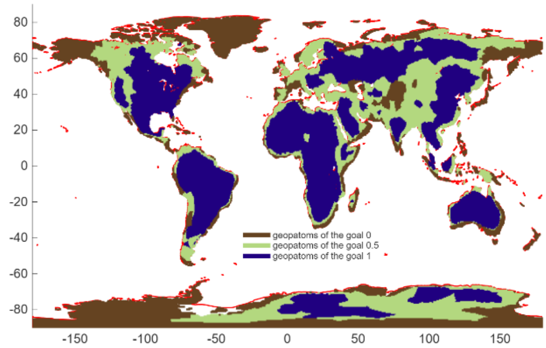

Figure 13b: Division of the geopatoms ensemble into three groups

Comparing the maps in Figure 13a and Figure 13b reveals that the center's geopatoms return to target group 0 when dividing the entire geopatoms ensemble into two groups. Conversely, when classifying into three groups, the target group 0.5 geopatoms emerges from group 0. This is also confirmed by the distribution of geopatoms among groups. When classifying the geopatoms ensemble into two groups, the number of geopatoms was distributed as follows: $N_0 = 572$, $N_1 = 319$. When classifying into three groups, it turned out that $N_0 = 250$, $N_{0.5} = 322$, $N_1 = 319$.

From this point on, everything is ready for the connection between geopolitics and psyphysics. The next three sections are devoted to laying out the fundamentals of psyphysics as they apply to our task of describing psychodynamics in geopolitics.

SUBJECT-OBJECT REALITY OF GEOPATOM

In the model of psyphysics, which has the subtitle "towards a theory of the interaction between the operator and the device", five definitions are introduced, answering the following questions: what is a device (two definitions), what is a psyatom, and what is an operator (two definitions)? Roughly speaking, an operator is someone (something) who (what) controls the device. The interaction between the operator and the device is interpreted from the perspective of the operator's control and power over the device. The operator itself is constructed in terms of will, freedom, force, and power. All four concepts — "will", "freedom", "force", and "power" — are defined and quantified in the model of psyphysics.

Following the logic of the psyphysics model, we will digitize the choice of two goals for each geopatom in the global geopolitical system. We will define the subjective space of all possible goals for a geopatom by the interval $[0,1]$. In this case, the geopatoms' choice

x is a number from the interval $[0,1]$, i.e., $x \in [0,1]$. We will agree that the choices $x = 0$ and $x = 1$ correspond to the choice of the realms of freedom and necessity, respectively. All other values $x \in (0,1)$ correspond to other subjective meanings of choice. We will assume that, in addition to the subjective reality of choice, there is an objective reality, which we will also digitize by the interval $[0,1]$. We will denote by the symbol X the manifestation of subjective choice in objective reality, and it is assumed that $X \in [0,1]$.

Following V.A. Lefebvre [11], we define the relationship between the subjective and objective realities of each geopatom using the function ϕ, i.e., we assume that $X = \phi(x)$. By definition, we assume that the function $\phi(x)$ is monotonically increasing on the interval $[0,1]$ and satisfies the following set of requirements:

$$\phi(0) = 0,\ \phi(1) = 1,\ \phi(x) + \phi(1 - x) = 1. \tag{22}$$

In what follows, by goals we will mean those points x_* of the segment $[0,1]$ at which the equality $\phi(x_*) = x_*$ holds. From this point of view, in addition to the goal points 0, 1, there is, at a minimum, one more goal point 0.5. It is obtained from the third equation in (22) by direct substitution $x = 0.5$. In this case, we have $\phi(0.5) = 0.5$. The third equation in (22) ensures complete symmetry between the pair of goals 0 and 1.

To further refine the form of the function $X = \phi(x)$, we need to determine the derivatives at the target points 0, 1, 0.5. The derivatives $\phi'(0)$, $\phi'(1)$, $\phi'(0.5)$ determine the rate of convergence to the target points 0, 1, 0.5 under reflexive closure or within the iterative procedure $x_{n+1} = \phi(x_n)$, $n = 0,1, \ldots$ We introduce a non-negative force parameter f, $f \in [0, +\infty)$ according to the following conditions:

$$\phi'(0) = \phi'(1) = \tfrac{1}{1+f},\ \phi'(0.5) = 1 + f. \tag{23}$$

We will search for a suitable function $X = \phi(x)$ in the class of fractional linear functions. Taking into account the fulfillment of conditions (22), (23), we find:

$$\phi(x) = \begin{cases} \frac{x}{1+f-2fx}, 0 \le x \le 0.5; \\ \frac{-f+(1+2f)x}{1-f+2fx}, 0.5 < x \le 1. \end{cases} \tag{24}$$

In addition to the direct function $\phi(x)$, we also consider the inverse function $\phi^{-1}(x)$. The latter exists because the function $\phi(x)$ is, by definition, monotonically increasing. Taking into account (24), it is easy to write that

$$\phi^{-1}(x) = \begin{cases} \frac{(1+f)x}{1+2fx}, 0 \le x \le 0.5; \\ \frac{f+(1-f)x}{1+2f-2fx}, 0.5 < x \le 1. \end{cases} \tag{24′}$$

Note that for the inverse function $\phi^{-1}(x)$ the conditions similar to (22), (23) are true, namely: $\phi^{-1}(0) = 0$, $\phi^{-1}(1) = 1$, $\phi^{-1}(x) + \phi^{-1}(1 - x) = 1$, ${\phi^{-1}}'(0) = {\phi^{-1}}'(1) = 1 + f$, ${\phi^{-1}}'(0.5) = \frac{1}{1+f}$.

In the following, the functions $\phi(x)$ and $\phi^{-1}(x)$ will be called the direct and inverse mappings that connect the subjective and objective realities of each geopatom. Figure 14a shows the appearance of the direct and inverse mappings constructed according to (24), (24′).

Figure 14b shows an illustration of reflexive motion to the target points $0,\ 0.5,\ 1$ based on direct and inverse mappings. A uniform grid $0 = x_1 < x_2 < \cdots < x_N = 1$ is defined there and transition vectors are constructed: 1) from the point with coordinates $(x_i, \phi(x_i))$ to the point – $(\phi(x_i), \phi(\phi(x_i)))$ for the direct mapping and 2) from the point with coordinates $\left(x_i, \phi^{-1}(x_i)\right)$ to the point – $(\phi^{-1}(x_i), \phi^{-1}(\phi^{-1}(x_i)))$ for the inverse mapping, where $i = 1, \dots, N = 10^3$. Markers in the form of black dots indicate the beginning of the corresponding vectors.

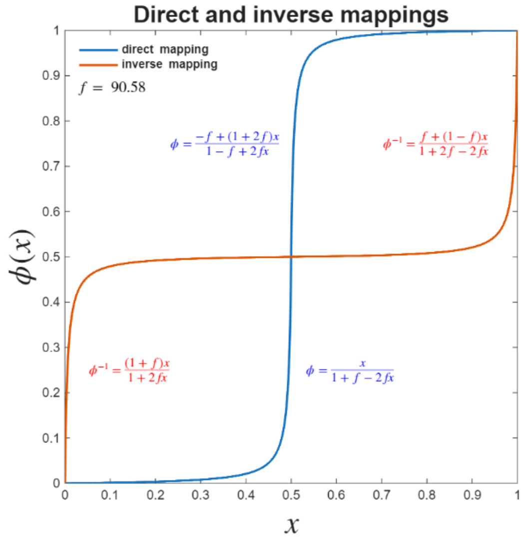

Figure 14a: External appearance of direct and inverse mappings

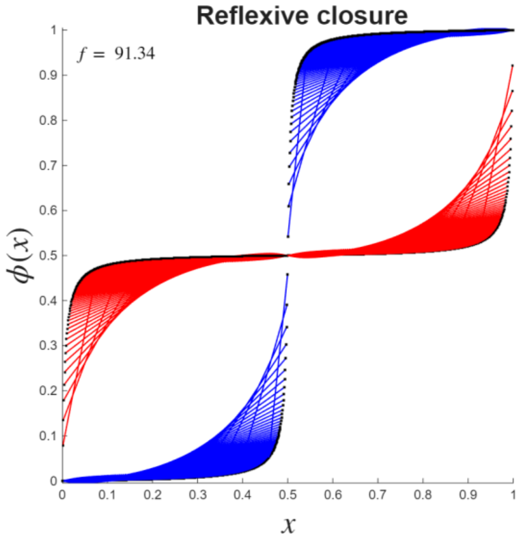

Figure 14b: Illustration of reflexive closure

As a result, we can conclude that the targets $0,\ 1$ are attracting, and the target 0.5 is repelling for the forward mapping $\phi(x)$. Conversely, the targets $0,\ 1$ are repelling, and the target 0.5 is attracting for the backward mapping $\phi^{-1}(x)$.

Let's introduce more convenient notations for the direct and inverse mappings ϕ_+ and ϕ_-, respectively. The subindex "+" symbolizes that targets 0 and 1 in the mapping ϕ_+ are attractive, while target 0.5 is repulsive. The subindex "−" means that targets 0 and 1 in the mapping ϕ_- are repulsive, while target 0.5 is attractive.

In what follows, we will need an analogue of the velocity in the target space $[0,1]$, or more precisely, two velocities $v_\pm$ for the pair of mappings $\phi_\pm(x)$. Note that if the pair of mappings $\phi_\pm(x)$ is considered as a function of two variables $\phi_\pm = \phi_\pm(x, f)$, then in the absence of force at $f = 0$ the mappings degenerate and become equal to x, i.e. $\phi_\pm(x, 0) = x$. In the latter case, there is no motion toward the target points in the target space. Thus, it is possible to speak of motion toward the target points only when the force is present, i.e., at $f > 0$.

To determine the speed of movement in the target space, we choose the expression:

$$v_\pm = v_\pm(x, f) = \phi_\pm(x, f) - x. \tag{25}$$

Let us write out the velocity (25) in more detail, taking into account the type of mappings $\phi_\pm(x, f)$ in (24), (24′). In this case, we obtain:

$$v_+ = \begin{cases} \frac{fx(-1+2x)}{1+f-2fx}, 0 \le x \le 0.5; \\ \frac{f(-1+2x)(1-x)}{1-f+2fx}, 0.5 < x \le 1; \end{cases} \tag{26}$$

$$v_- = \begin{cases} \frac{fx(1-2x)}{1+2fx}, 0 \le x \le 0.5; \\ \frac{f(2x-1)(x-1)}{1+2f-2fx}, 0.5 < x \le 1. \end{cases} \tag{26'}$$

Taking into account (22), (25), we can verify that $v_\pm(x) + v_\pm(1-x) = 0$. Figure 15 shows the graphs of the dependence of the velocities $v_\pm$ on x. We note a characteristic feature of the velocities defined in (25). The velocities in absolute value have a maximum value between the pair of targets 0, 0.5 and 0.5, 1, respectively. Moreover, for a sufficiently large value of the force parameter, the velocity reaches its maximum immediately after moving away from each of the target values. In Figure 15, the arrows indicate the directions of movement to the target points 0, 0.5, 1 for each of the two mappings.

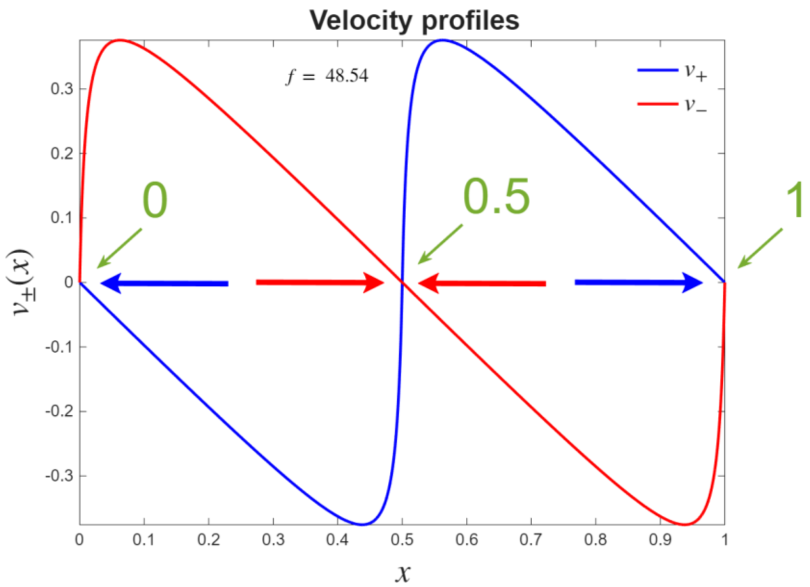

Figure 15: Graphs of the dependence of the velocities $v_\pm$ on x

PSYCHODYNAMICS OF AN ENSEMBLE OF INDEPENDENT GEOPATOMS

Let us consider an ensemble of N geopatoms. Let the subjective choice in the target space for each of them be characterized by the value x_i, where $x_i \in [0,1]$, $i = 1, \dots, N$. Following the model of psyphysics, we define the force parameter as the variation of the target preferences of the geopatoms in the ensemble, i.e.

$$f = \sum_{i=1}^{N} (x_i - \frac{1}{N} \sum_{j=1}^{N} x_j)^2 = \sum_{i=1}^{N} x_i^2 - \frac{1}{N} (\sum_{j=1}^{N} x_j)^2. \tag{27}$$

The force parameter defined according to (27) is equal to zero when $x_1 = x_2 = \dots = x_N$, i.e. when the subjective choice of each geopatom is united. The unity of geopatoms will further be represented as the fulfillment of the following condition: $\min_{1 \le i \le N} x_i = \max_{1 \le i \le N} x_i$.

Let us formulate the psychodynamics of the geopatoms ensemble in the target space in the following form:

$$\begin{cases} x_i' = \phi_{\pm}(x_i, f), \\ f = \sum_{i=1}^{N} x_i^2 - \frac{1}{N}(\sum_{j=1}^{N} x_j)^2. \end{cases} \tag{28}$$

The transition $x_i \to x_i'$, $i = 1, \dots, N$, according to (28), defines the psychodynamics of geopatoms in the target space. In the author's previous works [3], this transition was interpreted as a reflexive closure of each of the ensemble's geopatoms. A discrete variable $t = 0, \pm 1, \dots$ could be introduced, which can be interpreted as an analogue of time. In this case, $x_i = x_i(t)$, $x_i' = x_i(t+1)$, $i = 1, \dots, N$, and after the transition to the limit, when $t \to \infty$, each of the ensemble's geopatoms will arrive at one of the three target points 0, 0.5, 1.

To extend the psychodynamics beyond reaching one of the target states, it is necessary to define a procedure for exiting the target state. This procedure presupposes the presence of the will to exit targets 0, 0.5, and 1 in each geopatom. We introduce a notation for the volitional values (impulses) to exit each target state for each geopatom according to the expressions: $\delta_{0,i}$, $\delta_{0.5,i}$, $\delta_{1,i}$, $i = 1, \dots, N$.

The set of characteristics of each geopatom introduced above and below could be described, among other things, in terms of agent systems developed on the basis of AI [12].

Since each of the geopatoms can remain in any of the target states indefinitely, to exit it must 1) change the mapping to the opposite, i.e. $\phi_{\pm} \to \phi_{\mp}$ and 2) take, arbitrarily, a small but non-zero first step from each of the three goals, namely $\delta_{0,i}$, $\delta_{0.5,i}$, $\delta_{1,i}$, $i = 1, \dots, N$, respectively. Note that the volitional effort $\delta_{0.5,i}$ at the target point 0.5 has a sign, which subsequently implies either arriving at goal 0 when $\delta_{0.5,i} < 0$, or arriving at goal 1 when $\delta_{0.5,i} > 0$. The presence of a sign in the volitional impulse $\delta_{0.5,i}$ acts as a prototype of freedom in the form of a choice between two possibilities. Note that by definition, volitional impulses $\delta_{0,i}$, $\delta_{1,i}$, $i = 1, \dots, N$ are always non-negative, i.e. $\delta_{0,i} \geq 0$, $\delta_{1,i} \geq 0$, $i = 1, \dots, N$.

We need volitional impulses to determine the mechanism by which individual geopatoms in the ensemble unite into alliances. We'll assume that the volitional impulses of individual geopatoms are independent of each other and are completely chaotic in their manifestations. To conduct the computational experiment, we'll determine the criterion for reaching each of the three target states 0, 0.5, 1 according to the following inequalities:

$$x < \rho,\ |0.5 - x| < \rho,\ 1 - x < \rho, \tag{29}$$

where ρ is a sufficiently small non-negative number.

Let the volitional impulses in each of the three target states be represented as follows:

$$\delta_0 = \varepsilon\xi_0,\ \delta_{0.5} = \varepsilon(2\xi_{0.5} - 1),\ \delta_1 = \varepsilon\xi_1, \tag{30}$$

where ε is a sufficiently small non-negative number, and $\xi_0, \xi_{0.5}, \xi_1$ are uniformly random numbers from the interval $[0,1]$. The combination $(2\xi_{0.5} - 1)$, $\xi_{0.5} \in [0,1]$ in (30) ensures a uniformly random selection of the volitional impulse signs at the target point 0.5.

Taking into account (27) — (30), we write the following system of equations describing the psychodynamics of the ensemble of geopatoms:

$$f = \sum_{i=1}^{N} x_i^2 - \frac{1}{N}\left(\sum_{j=1}^{N} x_j\right)^2,$$

$$\tau_i' = +, x_i' = \phi_+(x_i, f)|_{\tau_i = +, x_i \geq \rho, x_i \leq 1-\rho};$$

$$\tau_i' = -, x_i' = \phi_-(x_i, f)|_{\tau_i=-,|0.5-x_i|\geq\rho};$$
$$\tau_i' = -, x_i' = \varepsilon\xi_i|_{\tau_i=+,x_i<\rho}; \tag{31}$$
$$\tau_i' = +, x_i' = 0.5 + \varepsilon(2\xi_i - 1)|_{\tau_i=-,|0.5-x_i|<\rho};$$
$$\tau_i' = -, x_i' = 1 - \varepsilon\xi_i|_{\tau_i=+,x_i>1-\rho};$$

where $i = 1, \ldots, N$, the quantities τ, τ' take two values "+" or "−", which denote the direct and inverse mappings, respectively. The vertical bar, together with a series of conditions in the subindices in (31) and below, denotes the conditions under which the equality sign holds.

Note that since the value of ρ in (29) is small but not zero, the dynamics based on the system of equations (31) will lead each of the geopatoms to one of the target points in a finite number of steps. The latter statement is true as long as among the set of geopatoms positions $x_1, \ldots, x_N$ there are at least two that are distinct from each other, i.e., as long as $\min_{1\leq i\leq N} x_i \neq \max_{1\leq i\leq N} x_i$ or, in other words, the force parameter is nonzero, i.e., $f \neq 0$.

Figure 16 shows an example of calculating the system of equations (31) within the framework of the reflexive closure procedure $x_i \to x_i'$, $\tau_i \to \tau_i'$, $i = 1, \ldots, N$ with the number of iterations, T, equal to $T = 10^4$. It was assumed that $N = 10^2$, $\rho = 10^{-12}$, $\varepsilon = 10^{-8}$.

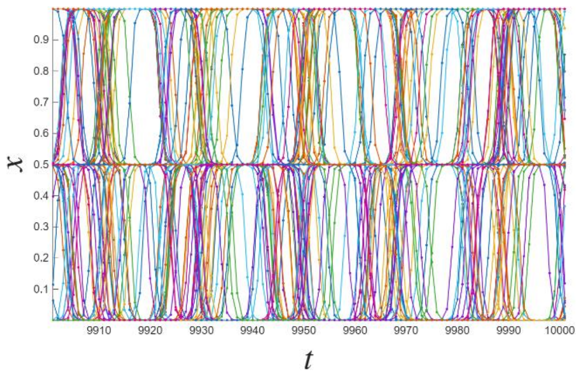

Figure 16a: A small fragment of the dynamics of the geopatoms ensemble in the target space

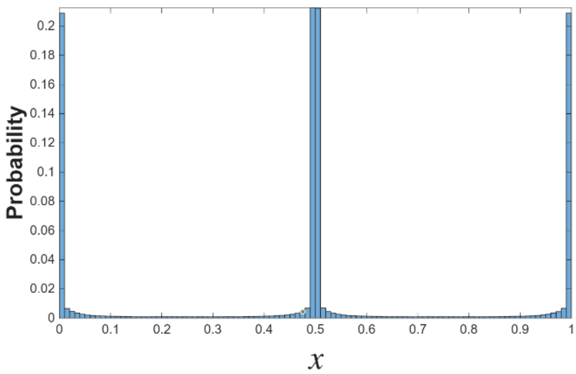

Figure 16b: Probability of geopatoms being present at points in the target space

Figure 16a shows a small fragment of the final dynamics of the geopatoms' ensemble in the target space. The start was made with random initial data. The figure depicts sets of point trajectories for each geopatom, connected by straight lines for convenience, resembling the trajectories of each geopatom in the target space. It is clear that the trajectories are entangled, and the geopatoms wander within the target space. This is expected, as the volitional impulses of the geopatom ensemble are independent of each other.

Using the same initial parameters as for the calculation in Figure 16a, Figure 16b evaluates the probabilities of geopatoms being in the vicinity of points in the target space using the corresponding histogram with 100 columns. It is evident that geopatoms are significantly likely to be in the vicinity of one of the three targets 0, 0.5, 1 and significantly less likely to be at intermediate points.

PSYCHODYNAMICS OF THE FORMATION OF GEOPATOMS' ALLIANCES

Let us consider several scenarios for the formation and movement of geopatoms' unions in the target space.

Let geopatoms interact with each other to form alliances. We assume that the number of alliances coincides with the number of target points, of which there are three: 0, 0.5, and 1. Let us denote the number of geopatoms affiliated with each of the three targets as N_0, $N_{0.5}$, and N_1, where $N = N_0 + N_{0.5} + N_1$. Since geopatoms' movements outside of the target points are completely determined, interaction between geopatoms is possible only through variations in the magnitudes of volitional impulses. In this case, it is assumed that $\delta_{\mu,i} = \delta_{\mu,i}(x_1, \dots, x_N)$, $\mu = 0{,}0.5{,}1$, $i = 1, \dots, N$.

Let us denote the set of geopatoms numbers of the μ-th target by the symbol G_μ, where $|G_\mu| = N_\mu$, $\mu = 0{,}0.5{,}1$. Let us introduce in the target space the average position X_μ and average velocity V_μ of the geopatoms of the μ-th target, according to the formulas:

$$X_\mu = \frac{1}{N_\mu} \sum_{i \in G_\mu} x_i,\ V_\mu = \frac{1}{N_\mu} \sum_{i \in G_\mu} v_{\tau_i, i}, \tag{32}$$

where $\mu = 0{,}0.5{,}1$.

Scenario #1. To ensure the formation of geopatoms' unions, we assume that at the target points, individual geopatoms take the first step of leaving the target towards the middle position when it is outside the target position ($X_0 \neq 0$, $X_{0.5} \neq 0.5$, $X_1 \neq 1$) and is either at rest or moving away ($V_0 \geq 0$, $0 \leq V_{0.5} \geq 0$, $V_1 \leq 0$). To ensure the specified scenario, we assume that

$$\begin{gathered}
\delta_{0,i} = \begin{cases} \varepsilon \xi_i (X_0 > 0)(V_0 \geq 0), i \in G_0; \\ \varepsilon \xi_i, i \in G_{0.5} \cup G_1; \end{cases} \\
\delta_{0.5,i} = \begin{cases} -\varepsilon \xi_i, i \in G_0; \\ -\varepsilon \xi_i (X_{0.5} < 0.5)(V_{0.5} \leq 0), i \in G_{0.5}; \\ \varepsilon \xi_i (X_{0.5} > 0.5)(V_{0.5} \geq 0), i \in G_{0.5}; \\ \varepsilon \xi_i, i \in G_1; \end{cases} \\
\delta_{1,i} = \begin{cases} \varepsilon \xi_i, i \in G_0 \cup G_{0.5}; \\ \varepsilon \xi_i (X_1 < 1)(V_1 \leq 0), i \in G_1; \end{cases}
\end{gathered} \tag{33}$$

where $i = 1, \dots, N$. In (33), the expressions in parentheses are equal to one or zero when the corresponding inequalities are true or false, respectively.

Taking into account (31) – (33), we define the following system of equations describing the psychodynamics of the arrival of geopatoms at the targets they prefer.

$$f = \sum_{i=1}^N x_i^2 - \frac{1}{N} \left(\sum_{j=1}^N x_j \right)^2,$$

$$\tau_i' = +, x_i' = \phi_+(x_i, f)|_{\tau_i = +, x_i \geq \rho, x_i \leq 1-\rho};$$

$$\tau_i' = -, x_i' = \phi_-(x_i, f)|_{\tau_i = -, |0.5 - x_i| \geq \rho};$$

$$\tau_i' = -, x_i' = \varepsilon\xi_i (X_0 > 0)(V_0 \geq 0)|_{i\in G_0, \tau_i=+, x_i<\rho};$$
$$\tau_i' = -, x_i' = \varepsilon\xi_i|_{i\in G_{0.5}\cup G_1, \tau_i=+, x_i<\rho};$$
$$\tau_i' = +, x_i' = 0.5 - \varepsilon\xi_i|_{i\in G_0, \tau_i=-, |0.5-x_i|<\rho}; \tag{34}$$
$$\tau_i' = +, x_i' = 0.5 - \varepsilon\xi_i (X_{0.5} < 0.5)(V_{0.5} \leq 0)|_{i\in G_{0.5}, \tau_i=-, |0.5-x_i|<\rho};$$
$$\tau_i' = +, x_i' = 0.5 + \varepsilon\xi_i (X_{0.5} > 0.5)(V_{0.5} \geq 0)|_{i\in G_{0.5}, \tau_i=-, |0.5-x_i|<\rho};$$
$$\tau_i' = +, x_i' = 0.5 + \varepsilon\xi_i|_{i\in G_1, \tau_i=-, |0.5-x_i|<\rho};$$
$$\tau_i' = -, x_i' = 1 - \varepsilon\xi_i|_{i\in G_0\cup G_{0.5}, \tau_i=+, 1-x_i<\rho};$$
$$\tau_i' = -, x_i' = 1 - \varepsilon\xi_i (X_1 < 1)(V_1 \leq 0)|_{i\in G_1, \tau_i=+, 1-x_i<\rho}.$$

where $i = 1, \dots, N$.

Figure 17 shows an example of calculating the system of equations (34) under the condition that $N = 10^3$, $\rho = 10^{-12}$, $\varepsilon = 10^{-8}$. The initial distribution of geopatoms in the target space was chosen uniformly randomly. The geopatoms' preference for one of the three targets was also chosen uniformly randomly. In the given calculation, $N_0 = 301$, $N_{0.5} = 369$, $N_1 = 330$. Markers in the form of circles, hexagrams, and diamonds indicate the trajectories of geopatoms that prefer targets 0, 0.5, and 1, respectively. An unambiguous division of the set of geopatoms for each of the three targets is evident.

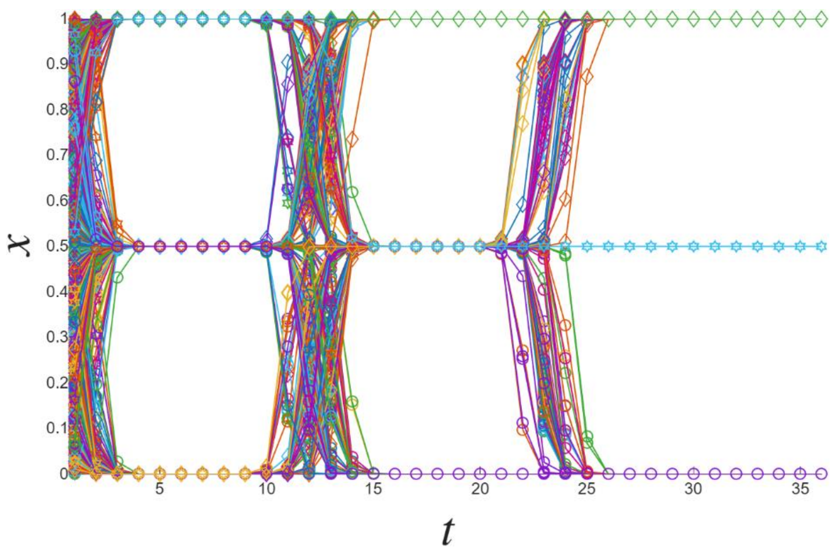

Figure 17: Scenario #1: dynamic distribution of geopatoms according to their preferred targets

As a result of psychodynamics, according to (34), all N geopatoms end up in each of their goals, with the final mappings "$-$", "$+$" and "$-$" corresponding to the required movement in the case of the first step exiting goals 0, 0.5, and 1, respectively, but now as geopatoms' unions. The geopatoms' unions formed as a result of the dynamics remain in the corresponding goal states and do not take their first steps.

Scenario #2. Let geopatoms, each favoring one of three goals, gather in one of them. In the author's model of psyphysics, such a configuration was called an operator. In this model, the term "union of geopatoms" is more appropriate. Generally, each i-th geopatom within the μ-th union has its own triplet of volitional impulses for each of the three target states, namely $\vartheta_{\lambda,i\in G_\mu}$; $\lambda,\mu = 0{,}0.5{,}1$. In this case, each union of geopatoms can move as a single entity within the target space. Let us clarify the type of volitional impulses of the geopatoms unions acting as a single whole, namely

$$\vartheta_{0,i} = \begin{cases} \varphi_{0,0}(\zeta_{0,0} < p_{0,0})\sigma_{0,0}, i \in G_0; \\ \varphi_{0,0.5}(\zeta_{0,0.5} < p_{0,0.5})\sigma_{0,0.5}, i \in G_{0.5}; \\ \varphi_{0,1}(\zeta_{0,1} < p_{0,1})\sigma_{0,1}, i \in G_1; \end{cases}$$

$$\vartheta_{0.5,i} = \begin{cases} \varphi_{0.5,0}(\zeta_{0.5,0} < p_{0.5,0})\sigma_{0.5,0}, i \in G_0; \\ \varphi_{0.5,0.5}(\zeta_{0.5,0.5} < p_{0.5,0.5})\sigma_{0.5,0.5}, i \in G_{0.5}; \\ \varphi_{0.5,1}(\zeta_{0.5,1} < p_{0.5,1})\sigma_{0.5,1}, i \in G_1; \end{cases} \quad (35)$$

$$\vartheta_{1,i} = \begin{cases} \varphi_{1,0}(\zeta_{1,0} < p_{1,0})\sigma_{1,0}, i \in G_0; \\ \varphi_{1,0.5}(\zeta_{1,0.5} < p_{1,0.5})\sigma_{1,0.5}, i \in G_{0.5}; \\ \varphi_{1,1}(\zeta_{1,1} < p_{1,1})\sigma_{1,1}, i \in G_1; \end{cases}$$

where is the set of ζ with subindices are uniformly random numbers from the interval $[0,1]$, $\sigma_{\lambda,\mu} = \prod_{k\in G_\mu}(x_k = \lambda)$; $\lambda,\mu = 0{,}0.5{,}1$.

The matrix $\varphi_{\lambda,\mu}$; $\lambda,\mu = 0{,}0.5{,}1$ has a size of 3×3, its elements denote the volitional impulses of the unions of geopatoms as a single whole, i.e. $\varphi_{\lambda,\mu}$ is the will of the μ-th union in the λ-th goal.

The matrix $\sigma_{\lambda,\mu}$; $\lambda,\mu = 0{,}0.5{,}1$, has a size of 3×3, and its elements take the pair of values 0 and 1. The value 0 means that the target geopatoms μ at the target point λ are not collected as a union. Conversely, the value 1 means that the target geopatoms μ at the target point λ are collected as a union.

Matrices $p_{\lambda,\mu}$, $\zeta_{\lambda,\mu}$; $\lambda,\mu = 0{,}0.5{,}1$ have size 3×3, the elements of the matrices are uniformly random numbers from the interval $[0,1]$. The elements of the matrix $\{p_{\lambda,\mu}\}$ have the meaning of the probabilities of the μ-th union leaving the target point λ.

Taking into account (35), it is necessary to slightly modify the volitional impulses (33), which describe the desire of geopatoms to unite into corresponding unions. We define the condition for the unity of geopatoms in the corresponding union as follows:

$$o_\mu = (\min_{k\in G_\mu} x_k = \max_{k\in G_\mu} x_k), \quad (36)$$

where $\mu = 0, 0.5, 1$. Note that the parentheses in expression (36) return either 1 if the equality is true, or 0 if the equality is false. Obviously, in the case where $o_\mu = 1$, all x_k, $k \in G_\mu$ coincide with each other, i.e. $x_{k_1} = \cdots = x_{k_{N_\mu}}$. In the case when $o_\mu = 0$, the multiple equality $x_{k_1} = \cdots = x_{k_{N_\mu}}$ is violated in one and/or more places.

Taking into account (36), we rewrite (33), then

$$\delta_{0,i} = \begin{cases} \varepsilon\xi_i(X_0 > 0)(V_0 \geq 0), i \in G_0; \\ \varepsilon\xi_i(o_{0.5} = 0), i \in G_{0.5}; \\ \varepsilon\xi_i(o_1 = 0), i \in G_1; \end{cases}$$

$$\delta_{0.5,i} = \begin{cases} -\varepsilon\xi_i(o_0 = 0), i \in G_0; \\ -\varepsilon\xi_i(X_{0.5} < 0.5)(V_{0.5} \le 0), i \in G_{0.5}; \\ \varepsilon\xi_i(X_{0.5} > 0.5)(V_{0.5} \ge 0), i \in G_{0.5}; \\ \varepsilon\xi_i(o_1 = 0), i \in G_1; \end{cases} \tag{37}$$

$$\delta_{1,i} = \begin{cases} \varepsilon\xi_i(o_0 = 0), i \in G_0; \\ \varepsilon\xi_i(o_{0.5} = 0), i \in G_{0.5}; \\ \varepsilon\xi_i(X_1 < 1)(V_1 \le 0), i \in G_1. \end{cases}$$

Taking into account (35) — (37), we write the following system of psychodynamic equations:

$$\begin{gathered} f = \sum_{i=1}^{N} x_i^2 - \frac{1}{N}\left(\sum_{j=1}^{N} x_j\right)^2, \\ \tau_i' = +, x_i' = \phi_+(x_i, f)|_{\tau_i=+, x_i \ge \rho, x_i \le 1-\rho}; \\ \tau_i' = -, x_i' = \phi_-(x_i, f)|_{\tau_i=-, |0.5-x_i| \ge \rho}; \\ \tau_i' = -, x_i' = \delta_{0,i}|_{i\in G_0, \tau_i=+, x_i<\rho} + \vartheta_{0,i}|_{i\in G_0, \tau_i=-, x_i<\rho}; \\ \tau_i' = -, x_i' = \delta_{0,i}|_{i\in G_{0.5}, \tau_i=+, x_i<\rho} + \vartheta_{0,i}|_{i\in G_{0.5}, \tau_i=-, x_i<\rho}; \\ \tau_i' = -, x_i' = \delta_{0,i}|_{i\in G_1, \tau_i=+, x_i<\rho} + \vartheta_{0,i}|_{i\in G_1, \tau_i=-, x_i<\rho}; \\ \tau_i' = +, x_i' = 0.5 + \delta_{0.5,i}|_{i\in G_0, \tau_i=-, |0.5-x_i|<\rho} + \vartheta_{0.5,i}|_{i\in G_0, \tau_i=+, |0.5-x_i|<\rho}; \\ \tau_i' = +, x_i' = 0.5 + \delta_{0.5,i}|_{i\in G_{0.5}, \tau_i=-, |0.5-x_i|<\rho} + \vartheta_{0.5,i}|_{i\in G_{0.5}, \tau_i=+, |0.5-x_i|<\rho}; \\ \tau_i' = +, x_i' = 0.5 + \delta_{0.5,i}|_{i\in G_1, \tau_i=-, |0.5-x_i|<\rho} + \vartheta_{0.5,i}|_{i\in G_1, \tau_i=+, |0.5-x_i|<\rho}; \\ \tau_i' = -, x_i' = 1 - \delta_{1,i}|_{i\in G_0, \tau_i=+, 1-x_i<\rho} - \vartheta_{1,i}|_{i\in G_0, \tau_i=-, 1-x_i<\rho}; \\ \tau_i' = -, x_i' = 1 - \delta_{1,i}|_{i\in G_{0.5}, \tau_i=+, 1-x_i<\rho} - \vartheta_{1,i}|_{i\in G_{0.5}, \tau_i=-, 1-x_i<\rho}; \\ \tau_i' = -, x_i' = 1 - \delta_{1,i}|_{i\in G_1, \tau_i=+, 1-x_i<\rho} - \vartheta_{1,i}|_{i\in G_1, \tau_i=-, 1-x_i<\rho}; \end{gathered} \tag{38}$$

where $i = 1, \dots, N$.

Figure 18a shows a typical example of calculating the system of equations (35) — (38). It was assumed that $T = 70$, $N = 10^3$, $N_0 = 332$, $N_{0.5} = 329$, $N_1 = 339$, $\rho = 10^{-12}$, $\varepsilon = 10^{-8}$. The matrix $\varphi_{\lambda,\mu}$; $\lambda, \mu = 0{,}0.5{,}1$ was chosen in the following form:

$$\{\varphi_{\lambda,\mu}\} = \varepsilon \begin{bmatrix} \eta_{0,0} & \eta_{0,0.5} & \eta_{0,1} \\ 2\eta_{0.5,0} - 1 & 2\eta_{0.5,0.5} - 1 & 2\eta_{0.5,1} - 1 \\ \eta_{1,0} & \eta_{1,0.5} & \eta_{1,1} \end{bmatrix}, \tag{39}$$

where the set η with subindices is uniformly random numbers from the interval $[0,1]$. Uniformly random numbers from the interval $[0,1]$ were chosen as the elements of the matrix $p_{\lambda,\mu}$, $\zeta_{\lambda,\mu}$; $\lambda, \mu = 0{,}0.5{,}1$.

According to the top graph in Figure 18a, all three types of geopatoms' alliances have formed. Markers were used to record their formation: a circle, a hexagram, and a diamond for targets 0, 0.5, and 1, respectively. Multiple repetitions of markers at target points reflect reduced probabilities of exiting the target points due to the random selection of the numerical values of the matrix elements $p_{\lambda,\mu}$; $\lambda, \mu = 0{,}0.5{,}1$. After the formation of geopatoms' alliances, their wandering in the target space is described by a random matrix of volitional impulses (39). Often, the dynamics quickly ceased, because three geopatoms' unions can easily meet in the target space, with a subsequent slowdown in dynamics when $f \to 0$ at $\min_{1 \le i \le N} x_i \leftrightarrow \max_{1 \le i \le N} x_i$. The tendency of the force value to zero is demonstrated by the lower graph in Figure 18a.

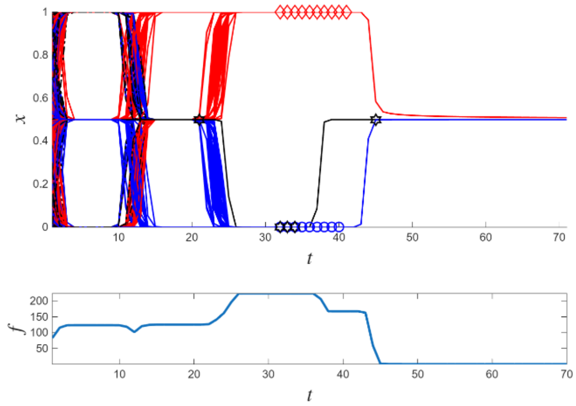

Figure 18a: Scenario #2: graphs of geopatoms dynamics in the target space (upper graph) and force (lower graph)

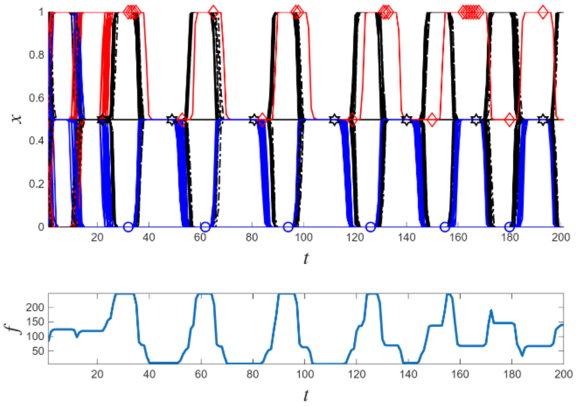

Figure 18b: Scenario #3: graphs of the dynamics of geopatoms in the target space (upper graph) and force (lower graph)

Thus, when each of the geopatoms unions is preserved, i.e. the geopatoms members of the unions are loyal to them and maintain the corresponding unity, the dynamics of movement in the target space quickly cease.

It should be noted, however, that the scenario for the formation of three geopatoms' alliances, presented in Figure 18a, has a significant flaw, as all three geopatoms' alliances are fundamentally indistinguishable from each other. The geopatoms' preferences for one of the three goals existed at the alliance formation stage, but once the alliances were formed, they became indistinguishable. More precisely, their volitional impulses, described by matrix (39), lack any specific goal preferences.

Scenario #3. Let's consider another scenario for the behavior of geopatoms' alliances that prioritize their own goals.

Let's assume that the geopatoms of goal 0 act independently after forming a union, i.e., they independently move from goal 0 to goal 0.5. In goal 0.5, they inevitably will goal 0. Thus, it turns out that the union of geopatoms of goal 0, as soon as it forms, ceases to exist. Then the mechanism for forming a union of geopatoms of goal 0 is activated, and the process repeats itself. This scenario demonstrates the geopatoms' preference for their own goal 0, which symbolizes the realm of freedom.

Geopatoms of target 0.5 do not linger at targets 0 and 1, as they are geopatoms of target 0.5. However, after forming an alliance at target 0.5, they act independently and can move to either target 0 or target 1. Under these circumstances, the alliance ceases to exist, and the mechanism for forming an alliance of geopatoms of target 0.5 is activated. Thus, the process repeats itself.

Geopatoms of goal 1 prefer the realm of necessity. We will assume that after the formation of a union of geopaths of goal 1, the union remains united even after its possible movement to goal 0.5. At goal 0.5, the union of geopaths inevitably chooses to return to goal 1. As a result, the union of geopatoms of goal 1, once formed, remains integral in the future.

Taking into account the stated assumptions, we reformat the volitional impulses of the unions of geopatoms (35) in the following form:

$$\vartheta_{0,i} = \begin{cases} \varepsilon\eta_i(\zeta_i < p_{0,0})\sigma_{0,0}, i \in G_0; \\ \varepsilon\eta_i(\zeta_i < p_{0,0.5})\sigma_{0,0.5}, i \in G_{0.5}; \\ \varphi_{0,1}(\zeta_{0,1} < p_{0,1})\sigma_{0,1}, i \in G_1; \end{cases}$$
$$\vartheta_{0.5,i} = \begin{cases} -\varepsilon\eta_i(\zeta_i < p_{0.5,0})\sigma_{0.5,0}, i \in G_0; \\ \varepsilon(2\eta_i - 1)(\zeta_i < p_{0.5,0.5})\sigma_{0.5,0.5}, i \in G_{0.5}; \\ \varphi_{0.5,1}(\zeta_{0.5,1} < p_{0.5,1})\sigma_{0.5,1}, i \in G_1; \end{cases} \quad (40)$$
$$\vartheta_{1,i} = \begin{cases} \varepsilon\eta_i(\zeta_i < p_{1,0})\sigma_{1,0}, i \in G_0; \\ \varepsilon\eta_i(\zeta_i < p_{1,0.5})\sigma_{1,0.5}, i \in G_{0.5}; \\ \varphi_{1,1}(\zeta_{1,1} < p_{1,1})\sigma_{1,1}, i \in G_1; \end{cases}$$

where $i = 1, \dots, N$, the values η with subindices are uniformly random numbers from the interval $[0,1]$.

In (40), the triplet of volitional impulses $\varphi_{0,1} = \varepsilon\eta_{0,1}$, $\varphi_{0.5,1} = \varepsilon\eta_{0.5,1}$, $\varphi_{1,1} = \varepsilon\eta_{1,1}$ is highlighted in color, where $\eta_{0,1}$, $\eta_{0.5,1}$, $\eta_{1,1}$ are uniformly random numbers from the interval $[0.1]$. The triplet of volitional impulses describes the movement of the union of geopatoms of target 1 in the target space. In addition, for the union of geopatoms of target 1, at each pass of one of the three targets, a triplet of uniformly random numbers $(\zeta_{0,1}, \zeta_{0.5,1}, \zeta_{1,1})$ from the interval $[0.1]$ is drawn.

Figure 18b shows a typical format of the ensemble geopatoms dynamics according to scenario #3. The graphs were obtained by solving the system of equations (37), (38), (40). It was assumed that $T = 200$, $N = 10^3$, $N_1 = 327$, $N_{0.5} = 345$, $N_1 = 328$, $\rho = 10^{-12}$, $\varepsilon = 10^{-8}$. As in Figure 18a, the markers in Figure 18b in the form of circles, hexagrams, and diamonds indicate the first steps of the exit of the unions of geopatoms of targets 0, 0.5, 1 from the corresponding target positions.

Note that solutions in the format shown in Figure 18b, i.e., quasi-periodic movements of the ensemble's geopatoms, can continue for quite a long time. If the number of geopatoms is less than ten, the dynamics may suddenly and rapidly cease. In this case, the geopatoms' positions in the target space will begin to converge, and the force will tend toward zero, i.e., $f \to 0$. Thus, a significant number of geopatoms (hundreds or more) ensure a long-term quasi-periodic dynamics regime in the target space.

Scenario #4. Within this scenario, we define a format for the dynamics of a geopatoms ensemble in which all geopatoms converge, then suddenly diverge, such that the force parameter reaches its maximum value. Maximum force is especially important in geopolitics, as, in the presence of weapons of mass destruction, it exerts a noticeable "psychophysical" impact on the behavior of geopatoms actors. This very scenario was previously considered in the author's work [13], devoted to studying the question: is the United Nations (UN), in terms of its activities over the past 50 years, nominal or real?

It's easy to see that the maximum force parameter f for a geopatoms ensemble N, $N \gg 1$, is $f_{\max} = \max_{x_1,\ldots,x_N \in [0,1]} f \approx \frac{1}{4}N$. Maximum force is achieved when the two halves of the entire geopatoms ensemble are maximally separated from each other in the target space. From the context, it's clear that the geopatoms of target 0.5 are not going to diverge between targets 0 and 1 to ensure maximum force. However, we can consider a situation where the geopatoms of the center are virtually absent.

Since the geopatoms' membership in one of the three targets was randomly selected when calculating the dynamics of the ensemble of geopatoms using equations (38), we define a triplet of probabilities $p_{tgt} = (p_{0,tgt}, p_{0.5,tgt}, p_{1,tgt})$. The components of the triplet p_{tgt} determine the probability of a geopatoms' membership in targets 0, 0.5, and 1, respectively, when they are initially assigned.

Figure 19 shows an example of calculating the system of equations (37), (38), (40). It was assumed that $T = 10^3$, $N = 10^3$, $N_0 = 510$, $N_{0.5} = 17$, $N_1 = 473$, $\rho = 10^{-12}$, $\varepsilon = 10^{-8}$, $p_{tgt} = (0.495, 0.01, 0.495)$.

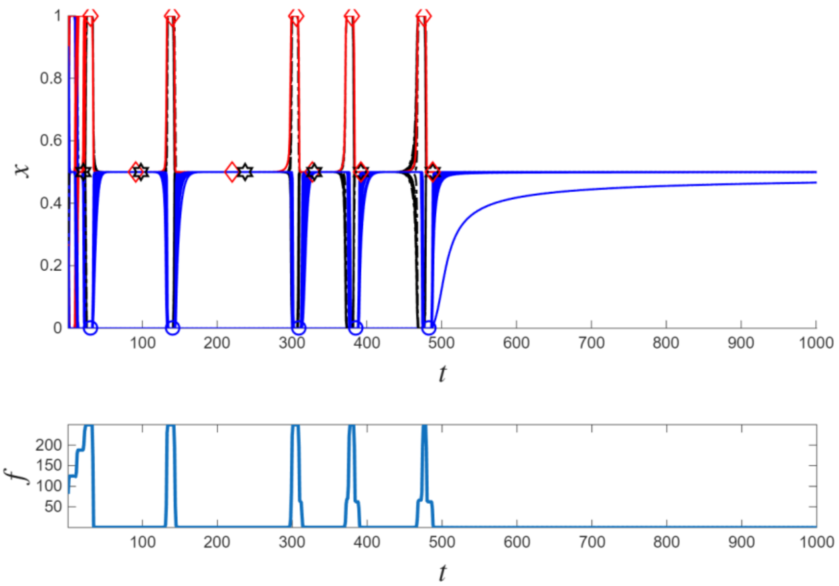

<u>Figure 19</u>: Scenario #4: geopatoms dynamics graphs in the target space (upper graph) and force (lower graph)

The type of dynamics presented in Figure 19 was ensured by choosing the probability matrix $p_{\lambda,\mu}$; $\lambda, \mu = 0, 0.5, 1$ close to the matrix of units J of size 3×3, i.e. $\{p_{\lambda,\mu}\} = 0.99 \cdot J + 0.01 \cdot R$, where R is a matrix of size 3×3, the elements of which are uniformly random numbers from the interval $[0,1]$. The proximity of the matrix $\{p_{\lambda,\mu}\}$ to the matrix of units J means that geopatoms practically do not linger in the target point when passing through it.

A characteristic feature of the geopatoms ensemble's behavior in scenario #4 is the flickering nature of its dynamics. The nearly fading dynamics ($f \to 0$) give way to a maximum increase in strength ($f \to f_{\max}$). Thus, five peaks of force growth can be observed in Figure

19. In the presented calculation, the maximum force was 249.7, which is very close to the maximum possible value of $f_{\max} = \frac{1}{4}N = 250$.

The above-discussed scenarios for the movement of a geopatoms ensemble in a target space led to the conclusion that there are two categories of movement. The first category of psychodynamics is characterized by an indefinitely ongoing dynamic; the second category, the dynamic can cease when the geopatoms positions in the target space converge, and the force parameter $f \to 0$. It should be noted that the possibility of the second category of movement fundamentally distinguishes psychodynamics from ordinary temporal dynamics.

THE COMBINATION OF GEOPOLITICS AND PSYCHOPHYSICS

Let us move on to the synthesis of models of geopolitics and psychophysics, which are presented in sections #2 — #7 and #8 — #10, respectively.

In section #7, the Earth's surface is divided into $N = 891$ parts, suitable for further model construction. Furthermore, for each of the $N = 891$ territories, the average weight $\overline{w}_i$, $i = 1, \ldots, N$, is calculated. This weight takes a value from the interval $[0,1]$ and denotes the territory's membership in low- to high-rank clusters. Weight values close to zero characterize the territory's membership in low-rank clusters, while values close to one characterize the territory's membership in high-rank clusters. Also in Figure 13, using cluster analysis, the division of the entire geopatoms ensemble into two (Figure 13a) and three (Figure 13b) groups, respectively, is shown.

Let's calculate the average weight of geopatoms in each of the groups. We introduce the notation for the average weight of geopatoms in each of the three groups, namely $W_\mu = \frac{1}{N_\mu}\sum_{i \in G_\mu} \overline{w}_i$, $\mu = 0{,}0.5{,}1$. In the previous section, we already introduced suitable notations for the set of geopatoms group numbers G_μ, $\mu = 0{,}0.5{,}1$ and the number of geopatoms in groups $N_\mu = |G_\mu|$, $\mu = 0{,}0.5{,}1$, while the equality $N_0 + N_{0.5} + N_1 = N = 891$ must be true.

Table 1 summarizes the number and average weight of geopatoms in groups. As noted in section #7, when moving from two to three groups, the group of geopatoms for target 0.5 is distinguished from the geopatoms for target 0. Note also that the average weights of geopatoms for targets 0 and 0.5 are closer to zero and differ significantly from the average weight of geopatoms for target 1.

Table 1: Number of geopatoms and average weight in groups

Number of groups	N_0/W_0	$N_{0.5}/W_{0.5}$	N_1/W_1
2	572/0.245	0/0	319/0.688
3	250/0.091	322/0.365	319/0.688

Let us further consider two scenarios of the dynamics of the ensemble of geopatoms in sequence: first for three groups, then for two groups.

Scenario #5. Let the geopatoms' ensemble be divided into three geopatoms' groups in a proportion corresponding to the second row of Table #1. Let's keep the numbering of the scenarios from the previous section going.

Let's define the probability matrix $p_{\lambda,\mu}$ of the exit of a union of geopaths of the μ-th target from the λ-th target point using the following formula:

$$p_{\lambda,\mu} = |\lambda - W_\mu|, \tag{41}$$

where $\lambda, \mu = 0{,}0.5{,}1$. The meaning of (41) is as follows. The probability of the μ-th union of geopatoms exiting the λ-th target point is zero when $\lambda = W_\mu$, i.e., when the geopatoms in the union are united in their choice and are located precisely at the target they prefer. If the latter equality is not satisfied, the union of geopatoms may exit one or another target where it is currently located.

Taking into account (41), as well as the average values of the weights $\{W_\mu\} = (0.091{,}0.135{,}0.312)$ of the geopatoms groups presented in the last row of Table #1, we find that

$$\{p_{\lambda,\mu}\} = \begin{bmatrix} 0.091 & 0.365 & 0.688 \\ 0.409 & 0.135 & 0.188 \\ 0.909 & 0.635 & 0.312 \end{bmatrix}. \tag{41′}$$

Note that, according to the (41′) matrix, the geopatoms alliances of targets 0, 0.5, and 1 have exit probabilities of 0.091, 0.135, and 0.312, respectively, from the same target points. Moreover, the exit probability of the geopatoms alliance of target 1 from the same target point is significantly greater than the similar probabilities of targets 0 and 0.5. These probabilities are highlighted in the (41′) matrix.

Figure 20a shows the results of calculating the dynamics of the ensemble of geopatoms by solving the system of equations (38), in which the volitional impulses to form alliances and, in fact, the geopatoms' alliances themselves corresponded to the choice of (37), (40), respectively. In terms of the format for selecting the volitional impulses of geopatoms' alliances, scenario #3 from the previous section was selected. A new aspect was the use of a specific probability matrix of exiting the target points (41′). It was assumed that $T = 250$, $N = 891$, $N_1 = 250$, $N_{0.5} = 322$, $N_1 = 319$, $\rho = 10^{-12}$, $\varepsilon = 10^{-8}$. The start was carried out from random positions of geopatoms in the target space.

An examination of Figure 20a leads to the following conclusions. All three geopatoms' alliances form fairly quickly and then continue to exist as isolated manifestations. Alliances, as above, are designated by markers in the form of circles, hexagrams, and diamonds for targets 0, 0.5, and 1, respectively. A single geopatoms alliance for target 1 manifests itself at two target points: 0.5 and 1. This precisely corresponds to scenario #3, discussed in the previous section, in which the geopatoms alliance for target 1, once formed, continues to move as a single entity. The latter property is not characteristic of geopatoms alliances for targets 0 and 0.5. Calculations for periods up to $T = 10^5$ revealed a uniform quasi-periodic pattern of geopatoms ensemble dynamics in the target space, while the variability of the force parameter significantly does not reach the maximum, equal to the value $f_{max} \cong \frac{N}{4} = 222.75$.

Considering the quasi-periodic nature of the geopatoms ensemble dynamics, shown in Figure 20a, we find the weighted average position of each geopatom in the target space. We introduce the following notation for the average geopatom positions:

$$\bar{x}_i = \frac{1}{T-t_0} \sum_{t=t_0+1}^{T} x_i(t), \tag{42}$$

where $i = 1, \ldots, N$, and t_0 is the period of establishment of the quasi-periodic dynamic's regime. Thus, Figure 20a shows that the establishment period is less than the value $t_0 = 50$.

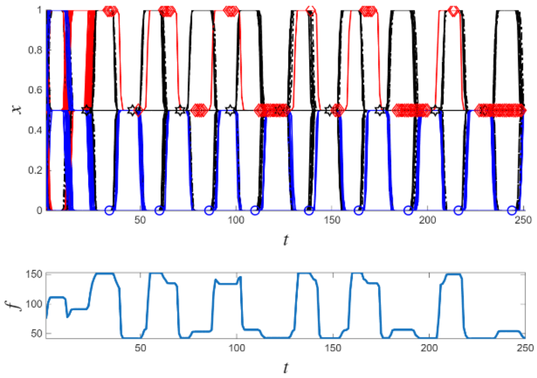

Figure 20a: Scenario #5: graphs of geopatoms dynamics in the target space (upper graph) and force (lower graph)

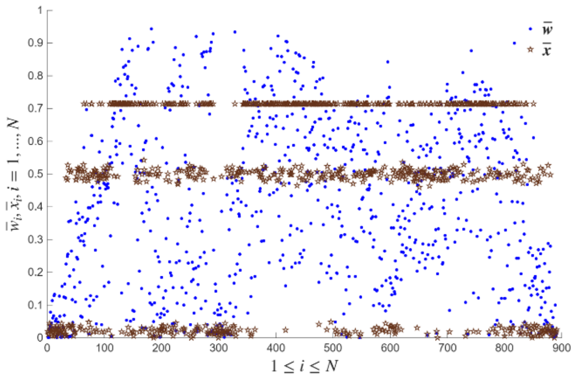

Figure 20b: Comparison of average weights and average positions of the ensemble geopatoms in the target space

Figure 20b compares two distributions for the geopatoms' ensemble: average weights (depicted as dots) and average positions in the target space (depicted as pentagrams), found according to (42). It was assumed that $T = 10^3 + 50$, $t_0 = 50$. The figure clearly shows that the average weights, characterizing the geopatoms' belonging to low- and high-rank clusters, are quasi-uniformly randomly distributed in the target space. The geopatoms' average positions over time in the target space are concentrated in the form of distinct bands, which were previously interpreted as groups of geopatoms of targets 0, 0.5, and 1. The lack of variability in the target position of geopatoms of target 1 is due to the fact that the union of geopatoms of target 1, having once emerged, continues to exist.

In full accordance with the psyphysics model, each geopatoms in the ensemble identified its affiliation with one of three targets. Moreover, the identified target separation in some cases occurred not because of, but in spite of, the geophysical foundations of a given geopatom. The average weight of a geopatoms serves as this geophysical foundation. Thus, each i-th geopatom is situated between its own geophysical foundation, represented by the value $\bar{w}_i$, on the one hand, and the current psyphysical situation, represented by the value $\bar{x}_i$, on the other.

In examining the next scenario with two groups of geopatoms in the target space, we note the following consideration. Scenario #4 from the previous section was specifically considered because it leads to a flickering psychodynamic pattern. In this pattern, long periods of near-zero force values alternate with a sharp increase up to a maximum, followed by a subsequent rebound to low force values. This pattern is important for studying the termination of psychodynamics in the target space, when all geopatoms are in the vicinity of the same target, and force tends toward zero. This pattern contrasts sharply with the previous scenario, in which the psychodynamics was quasi-periodic and lasted for a significant number of iterations.

Scenario #6. Let the geopatoms' ensemble be divided into two geopatoms' groups in a proportion corresponding to the first row of Table #1.

We now follow the logic of scenario #4 from the previous section. The type of dynamics shown in Figure 19 was achieved by selecting the probability matrix $p_{\lambda,\mu}$; $\lambda,\mu = 0{,}0.5{,}1$, close to the 3×3 matrix of units J. We choose $\{p_{\lambda,\mu}\} = 0.9925\cdot J + 0.0075\cdot R$, where R is a 3×3 matrix whose elements are uniformly random numbers from the interval $[0{,}1]$. The proximity of the matrix $\{p_{\lambda,\mu}\}$ to the matrix of units J means that geopatoms practically do not linger in the target point when passing through it.

Figure 21a shows a sample of flickering dynamics in the target space of the geopatoms' ensemble. It was assumed that $T = 10^3$, $N = 891$, $N_0 = 572$, $N_1 = 319$, $\rho = 10^{-12}$, $\varepsilon = 10^{-8}$. The upper graph showed seven oscillations from a force value close to zero to a maximum value, equal in this calculation variant to $f_{max} = \frac{N_0 N_1}{N_0 + N_1} \cong 204.79$. The nature of the force variability is shown in the lower graph.

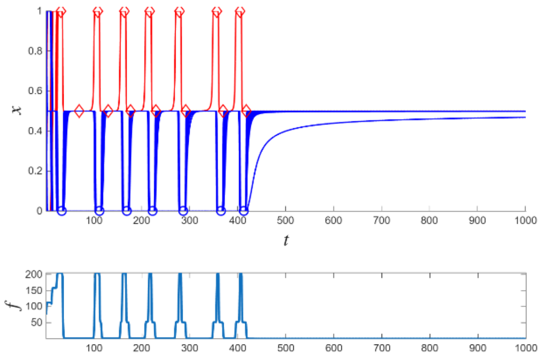

Figure 21a: Scenario #6: graphs of geopatoms dynamics in the target space (upper graph) and force (lower graph)

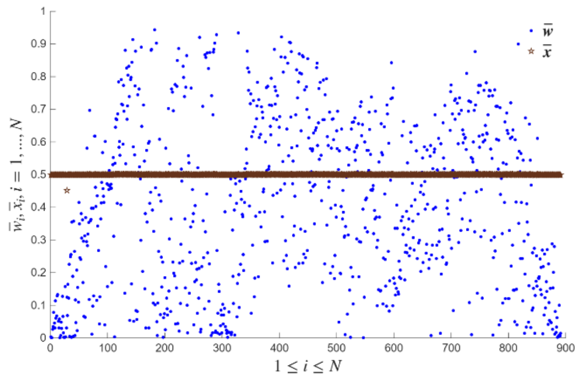

Figure 21b: Comparison of average weights and average positions of ensemble geopatoms in the target space

Figure 21b shows the joint positioning of the average weights of geopatoms, as well as the average positions of the ensemble geopatoms, calculated according to formula (42). We assumed that $T = 10^3$, $t_0 = 500$, $N = 891$, $N_0 = 572$, $N_1 = 319$, $\rho = 10^{-12}$, $\varepsilon = 10^{-8}$. Since all geopatoms of the ensemble are concentrated in the vicinity of the target point 0.5, their average positions over the last $T - t_0 = 500$ iterations turned out to be close. If in Figure 20b the groups of geopatoms of the corresponding targets are well defined, i.e., spread out in the target space, in Figure 21b the geopatoms of targets 0 and 1 are not separated from each other, being in the vicinity of the target point.

Note that the prolonged approach to target point 0.5 in Figure 21b may be followed by a sudden, sharp dispersal of geopatoms toward targets 0 and 1, followed by a repeated approach to target 0.5. It is precisely this mode of prolonged convergence of all geopatoms in an ensemble toward one of the target points (usually toward target point 0.5) that was considered in the normative model of global history [13] as one of the scenarios for the completion of global historical psychodynamics. Overall, Figure 21b demonstrates the triumph of psyphysics over geophysics. While from a geophysical perspective, all geopatoms are distinct, from a psyphysical perspective, they are identical in the vicinity of a single target point.

PSY(GEO)PHYSICAL CONTEXT OF THE POLITICAL MAP OF THE WORLD

From the last section, it became clear that behind the facade of global psyphysical variability, represented by psychodynamics, lies something more or less invariant and relatively unchangeable — the geophysical peculiarity of a given geopatom. This peculiarity can be described in terms of climate, topography, and traffic, as has been previously explored in the author's works [1,2] using the example of a mathematical model of geopolitics.

As a result, the global political map of the world can be viewed simultaneously from two perspectives — psyphysical and geophysical. In other words, it is necessary, using the example of the current political map of the world, to understand what is more (less) in the existence of states — psyphysics or geophysics.

In section #3, we already considered a basic grid on the surface of the globe with a resolution of half a degree. The total number of such grid nodes is $N_{Sphere} = 360 \times 720 = 259'200$. After subtracting the points attributed to the ocean surface, we found the number of land surface points to be $N_{Land} = 81'192$. Let's assign all land nodes to a particular state. Let's assume the number of states (as well as territories with other statuses) on Earth is N_c. Then, each state can be associated with sets of points $C_i,\ i = 1, \dots, N_c$, from the set N_{Land}.

Section #7 defines $N_{lm} = 891$ clusters of land points $A_j,\ j = 1, \dots, N_{lm}$, which are considered local maxima of land surface point weights, classifying them in terms of low- to high-rank cluster preferences. Thus, N_{Land} land points can be divided into groups in two ways: 1) by country, $C_i,\ i = 1, \dots, N_c$, and 2) by their geophysical preferences, $A_j,\ j = 1, \dots, N_{lm}$.

We define a binary operation $g(C_i, A_j),\ i = 1, \dots, N_c,\ j = 1, \dots, N_{lm}$, between sets $\{C_1, \dots, C_{N_c}\}$ and $\{A_1, \dots, A_{N_{lm}}\}$, which returns the empty set when one set is completely contained in the other, is equal to the other, or is disjoint from the other, and the intersection of the pair of sets otherwise. In this case, we can write:

$$g(A,B) = \begin{cases} \emptyset, (A \subseteq B) \vee (A \supseteq B) \vee (A \cap B = \emptyset); \\ A \cap B, \overline{(A \subseteq B) \vee (A \supseteq B) \vee (A \cap B = \emptyset)}; \end{cases} \tag{43}$$

where $\vee$ is the logical operation "or" and the overbar is logical negation.

The meaning of operation (43) is as follows. When the corresponding pair of sets partially overlaps, a "tension" arises between the current political system and geophysics. The presence of tension is expressed by the fact that $g(C_i, A_j) \neq \emptyset$ for given i, j. Conversely, when $g(C_i, A_j) = \emptyset$, one set is contained within the other, is equal to the other, or does not intersect the other.

Taking into account that operation (43) is symmetric with respect to the permutation of arguments, the following pair of sets of land point sets can be defined:

$$\mathcal{C}_i = \cup_{j=1}^{N_{lm}} g(C_i, A_j),\ i = 1, \dots, N_c; \tag{44}$$

$$\mathcal{A}_j = \cup_{i=1}^{N_c} g(A_j, C_i),\ j = 1, \dots, N_{lm}. \tag{44'}$$

The set $\mathcal{C}_i$, obtained using (44), consists of those points that correspond to the partial inclusion of one or more regions from the group $\{A_1, \dots, A_{N_{lm}}\}$ in the i-state. Overall, the set $\mathcal{C}_i$ can be interpreted as a collection of points of tension in the state structure, points where there is tension between psyphysics and geophysics. As a rule, these points are close to the state border of each state.

Similarly, the set $\mathcal{A}_j$, obtained using (44′), consists of those points that correspond to the partial inclusion of one or a group of states from the set $\{C_1, \dots, C_{N_c}\}$ in the j-th region. Since region $\mathcal{A}_j$ is not a state, we can speak of its development by one or a group of states, with the development sites located close to the boundary of the j-th region. In general, the set $\mathcal{A}_j$ can be interpreted as points of tension between a habitat without humans and a human-friendly environment with minimal infrastructure for life.

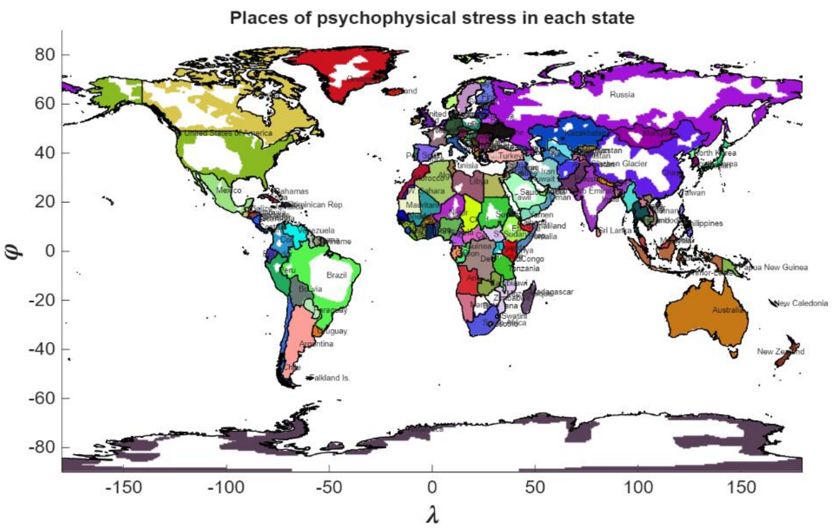

Figure 22: Political map of the world taking into account places of psychophysical stress

Figure 22 shows the boundaries of $N_c = 171$ states with the corresponding names. The boundaries are highlighted with a black line. Randomly colored territories from the set $\{A_1, \dots, A_{N_{lm}}\}$ that partially intersect the state border. White uncolored territories within Russia, China, Brazil, the USA, Canada, India, etc. denote territories from the set $\{A_1, \dots, A_{N_{lm}}\}$ that are completely included in the listed countries. Visual inspection of the map in Figure 22 revealed that Botswana and Zimbabwe do not have colored territories within their state borders. Thus, both countries have no psychophysical stress. Their existence is fully consistent with their individual geophysics.

Let's take a closer look at a map of the Russian Federation, highlighting areas requiring careful political monitoring and psychophysical stress. Figure 23a shows the desired map. It's worth noting the significant number of areas that require significant political monitoring to address potential centrifugal social forces.

A set of territories $\{\mathcal{A}_1, \dots, \mathcal{A}_{N_{lm}}\}$ was also found using formula (44′). It turned out that among the existing set, there is a single territory in the vicinity of Antarctica, in the region of the International Date Line. In Figure 23b, this territory is highlighted in color and also outlined by red ellipses. In addition, the graph shows the borders of states and their names, colored randomly. Thus, only one territory in Antarctica is not covered by the community of states on Earth.

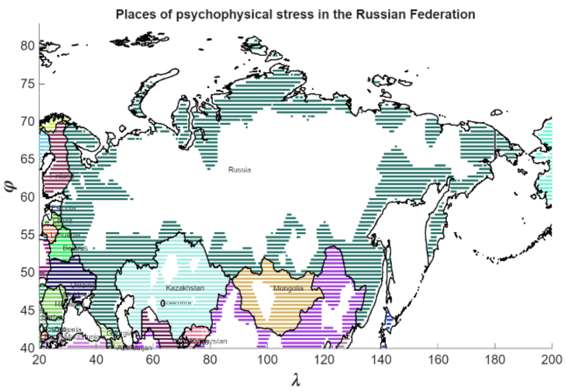

Figure 23a: The locations of psychophysical monitoring on the territory of the Russian Federation are highlighted in a single color

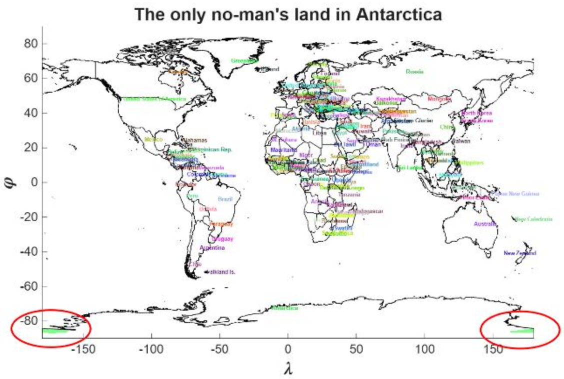

Figure 23b: The only territory in Antarctica in the International Date Line region that is not covered by states

Let's define the desired index, $I_{psy/geo,i}$, which evaluates the share of psychophysics in the structure of the i-th state, $i = 1, \dots, N_c$. We introduce the notation for the area of psychophysical stress points $P_i = mes\, \mathcal{C}_i$, $i = 1, \dots, N_c$ for each of the states. We also introduce the notation for the area of states $S_i = mes\, C_i$, $i = 1, \dots, N_c$. In this case, the desired index is represented as follows:

$$I_{psy/geo,i} = 100\% \frac{P_i}{S_i},\ i = 1, \dots, N_c. \tag{45}$$

The meaning of the index $I_{psy/geo,i}$ is as follows. It describes the role of politics in the structure of the i-th state. An additional index can also be introduced

$$I_{geo/psy,i} = 100(1 - \frac{P_i}{S_i}),\ i = 1, \dots, N_c. \tag{45′}$$

The index $I_{geo/psy,i}$ describes the share of geophysics in the structure of the i-th state. Obviously, $I_{psy/geo,i} + I_{geo/psy,i} = 100\%$, $i = 1, \dots, N_c$. Figure 24 shows the result of calculating index (45).

An analysis of the histogram in Figure 24 reveals the following characteristic features. Twenty states out of $N_c = 171$ were found to have a zero psychophysical index value, i.e., they are 100% geophysical formations. Finally, 13 states (taking into account rounding) have a psychophysical index value of 100%, i.e., they are 100% composed of politics. In Figure 24, in addition to the names of the states, the rounded values of the psychophysical index are displayed. The largest countries on the globe are highlighted in red: Russia, China, Brazil, the United States of America, Canada, and India, with index values of 40%, 45%, 46%, 52%, 54%, and 56%. All of these countries have index values around 50% and are equidistant from the extremes of zero and 100%.

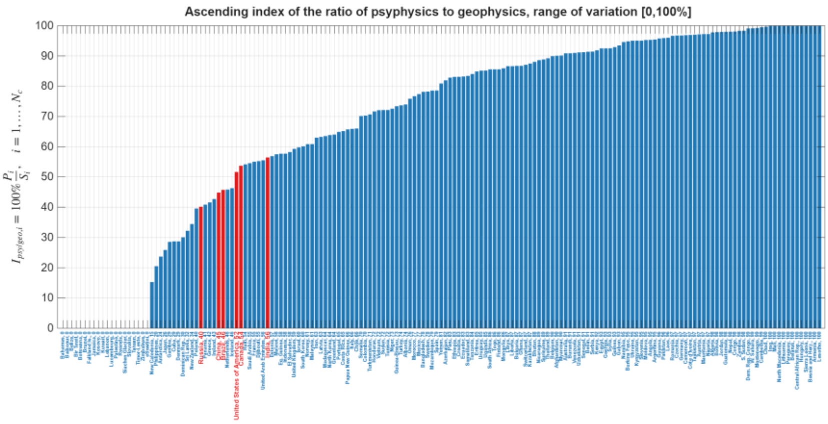

Figure 24: Final distribution of the index of the ratio of psyphysics and geophysics in ascending order

Figure 25 shows maps of the locations of territories that have 100% geophysics (Figure 25a) and 100% psyphysics (Figure 25b) in their devices.

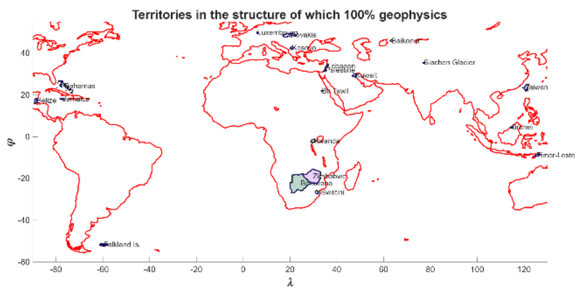

Figure 25a: 20 territories in the structure of which 100% geophysics

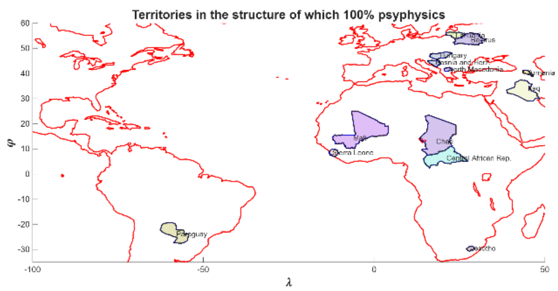

Figure 25b: 13 territories in the structure of which there is 100% psyphysics

Let's collect the index values (45), (45′) for all $N_c = 171$ countries. Table 2 contains the required data. The histogram data in Figure 24 and in Table 2 are completely consistent.

Let's estimate the global psy(geo)physics ratio for the entire globe. Taking into account (45), we write the following calculation formula:

$$I_{psy/geo} = 100\% \frac{\sum_{i=1}^{N} P_i}{\sum_{i=1}^{N} S_i}. \tag{46}$$

As a result, using formula (46), it was calculated that the global index was $I_{psy/geo} = 63.31\%$. In other words, in general, in the global world, politics significantly outweighs geophysics.

<u>Table 2</u>: Index values (45), (45′) by country

Country name	$I_{psy/geo}$	$I_{geo/psy}$
Bahamas	0	100
Baikonur	0	100
Belize	0	100
Bir Tawil	0	100
Botswana	0	100
Brunei	0	100
Falkland Is.	0	100
Jamaica	0	100
Kosovo	0	100
Kuwait	0	100
Lebanon	0	100
Luxembourg	0	100
Palestine	0	100
Rwanda	0	100
Siachen Glacier	0	100
Slovakia	0	100
Taiwan	0	100
Timor-Leste	0	100
Zimbabwe	0	100
eSwatini	0	100
New Caledonia	15	85
Philippines	20	80
Antarctica	24	76
Japan	26	74
Gambia	29	71
Cuba	29	71
Denmark	29	71
Dominican Rep.	30	70
Sri Lanka	32	68
New Zealand	34	66
Poland	40	60
Russia	40	60
Panama	41	59
Greece	42	58
Ireland	43	57
China	45	55
Brazil	46	54
Netherlands	46	54
Iceland	46	54
United States of America	52	48
Canada	54	46
Haiti	54	46
Saudi Arabia	55	45
France	55	45
Djibouti	55	45
United Arab Emirates	56	44
India	56	44
Estonia	57	43
Malawi	58	42
Eq. Guinea	58	42
Indonesia	58	42
El Salvador	58	42

United Kingdom	59	41
Israel	60	40
South Korea	60	40
Norway	61	39
Malaysia	61	39
Iran	63	37
Latvia	63	37
Madagascar	64	36
North Korea	64	36
Greenland	64	36
Portugal	65	35
Costa Rica	65	35
Papua New Guinea	66	34
Italy	66	34
Chile	66	34
Somalia	70	30
Colombia	70	30
Turkmenistan	71	29
Honduras	72	28
Vietnam	72	28
Sudan	72	28
Tunisia	72	28
Niger	73	27
Guinea-Bissau	73	27
Turkey	74	26
Albania	74	26
Oman	76	24
Morocco	77	23
Mexico	77	23
Bangladesh	78	22
Sweden	78	22
Mozambique	79	21
Spain	79	21
Yemen	81	19
Azerbaijan	82	18
Peru	83	17
Ethiopia	83	17
Croatia	83	17
Ecuador	83	17
Somaliland	83	17
Tanzania	84	16
Eritrea	85	15
Uruguay	85	15
Uganda	85	15
South Africa	86	14
Togo	86	14
Finland	86	14
Mongolia	86	14
Libya	87	13
Liberia	87	13
Bulgaria	87	13
Ghana	87	13
Switzerland	87	13
Kazakhstan	87	13
Bhutan	88	12

Nicaragua	89	11
Suriname	89	11
Thailand	89	11
Belgium	90	10
Afghanistan	90	10
Myanmar	90	10
Australia	91	9
Burundi	91	9
Venezuela	91	9
Uzbekistan	91	9
Senegal	91	9
Benin	91	9
Serbia	91	9
Kenya	92	8
Egypt	93	7
Georgia	93	7
Syria	93	7
Guinea	93	7
Gabon	93	7
Namibia	95	5
Burkina Faso	95	5
Ukraine	95	5
Kyrgyzstan	95	5
Slovenia	95	5
Moldova	95	5
Angola	95	5
Argentina	95	5
Guyana	96	4
Pakistan	96	4
Laos	96	4
Romania	97	3
Czechia	97	3
Germany	97	3
Cameroon	97	3
Côte d'Ivoire	97	3
Tajikistan	97	3
Austria	97	3
Mauritania	97	3
Nigeria	97	3
Algeria	98	2
Bolivia	98	2
Jordan	98	2
Guatemala	98	2
Nepal	98	2
Congo	98	2
Zambia	98	2
S. Sudan	98	2
Dem. Rep. Congo	99	1
W. Sahara	99	1
Montenegro	99	1
Cambodia	99	1
Chad	100	0
Iraq	100	0
Mali	100	0
North Macedonia	100	0

Lithuania	100	0
Paraguay	100	0
Belarus	100	0
Central African Rep.	100	0
Hungary	100	0
Sierra Leone	100	0
Bosnia and Herz.	100	0
Armenia	100	0
Lesotho	100	0

CONCLUSION

The presented mathematical model successfully combines geopolitics on the one hand and psyphysics on the other. The author had previously developed both the first and second mathematical models independently. The synthesis of these two models led to unexpected results.

From a geopolitical perspective, a justifiable division of the Earth's landmass was found. These territories were called geopatoms, and their selection was based on the locations of small- and large-ranking clusters of territories. The land division procedure took into account all standard geopolitical factors, such as climate, topography, and traffic.

From a psyphysical perspective, each identified geopatom was endowed with an internal goal space, parameterized by the interval $[0,1]$. Two global metahistorical goals, referred to in the normative model of global history as the realms of freedom and necessity, were defined within this goal space. These two goals were marked by points 0 and 1. In addition to these goals, a central goal, described by the number 0.5, was also introduced. All geopatoms were polarized based on their goal preferences. Global geopolitical psychodynamics refers to the study of patterns of movement in geopatoms' goal preferences.

Two types of geopatoms ensemble movement have been discovered and classified. One is an unbounded psychodynamic in the form of quasi-periodic oscillations. This corresponds to our physicalistic expectations of geopatoms wandering indefinitely in a target space. The second type of movement can lead to a halt in the psychophysical process, when all geopatoms meet at a single point for all purposes, typically at 0.5. Many initial configurations and specifically tuned parameters of the system as a whole lead to this second type of behavior. The interpretation of this second type of movement is open to multiple interpretations. It was not the purpose of this work to examine the various interpretations of this halt phenomenon.

Of particular note is the final section of the work, which reveals the psy(geo)physical context of the world's political map. A single psy(geo)physical index is introduced and calculated for all states on the planet. It ranges from $[0,100\%]$ and determines the percentage of psyphysics, or simply politics, in the structure of each state on Earth. The index was calculated for 171 states or territories with other statuses.

A study of the general statistics of the calculated index revealed that large countries such as Russia, China, Brazil, the United States, Canada, and India have index values around 50%. The index of most countries fluctuates widely, from very low values, literally 0%, to

100%. The calculated index has a double meaning: if subtracted from 100%, we obtain the geophysical index for each country's structure.

Finally, the psy(geo)physics index was calculated for the world as a whole. It turned out that for the world as a whole, it equals 63.31%, meaning that there is more psyphysics than geophysics in the structure of the world.

REFERENCES

1. Plokhotnikov K.E. Mathematical model of geopolitics, e-book. — Society for Science and Education. Promoting Education and Research, United Kingdom, 2018. — 66p. http://scholarpublishing.org/sse/wp-content/uploads/2018/08/ABR-4819.pdf
2. Plokhotnikov K.E. Definition of the Concept of Force in Geopolitics// Archives of Business Research, 2026, Vol.14, No.7, pp.12 – 37; https://doi.org/10.14738/abr.1407.11909
3. Plokhotnikov K.E. Eschatological strategic initiative: historical, political, psychological and mathematical commentary. — Moscow: Goryachaya Liniya – Telecom, 2014. — 251p. ISBN 978-5-9912-7006-9; https://www.techbook.ru/book.php?id_book=736
4. Plokhotnikov K.E. Normative Model of Global History// Global Journal of Science Frontier Research: A Physics and Space Science, 2022, Vol.22, Issue 5, Version 1.0, pp.33 – 59; https://globaljournals.org/GJSFR_Volume22/5-Normative-Model-of-Global.pdf (DOI: 10.17406/GJSFR) https://doi.org/10.34257/GJSFRAVOL22IS5PG33
5. http://climate.geog.udel.edu
6. http://climate.geog.udel.edu/html_pages/README.lw2.html
7. http://climate.geog.udel.edu/html_pages/README.lw.html
8. https://neo.gsfc.nasa.gov/view.php?datasetId=SEDAC_POP
9. Erlander S. The Gravity Model in Transportation Analysis: Theory and Extensions/ S. Erlander, N. F. Stewart. — Utrecht: VSP, 1990. — 226p.
10. James G., Witten D., Hastie T., Tibshirani R. An Introduction to Statistical Learning. 2nd ed. — Springer, 2021. — 607p.
11. Lefebvre V. Conflicting Structures. — Leaf & Oaks Publishers, 2015. — 144p.
12. Huyen, C. AI Engineering: Building Applications with Foundation Models. — Sebastopol: O'Reilly Media, 2025. — 350 p.
13. Plokhotnikov K.E. Mathematical Modeling of Global Social Dynamics/lecture course. — M.: Flinta, 2018. — 388p. — ISBN 978-5-9765-3945-7